THESIS FOR THE DEGREE OF DOCTOR OF PHILOSOPHY

Interactions between Wood Polymers in Wood Cell Walls and Cellulose/Hemicellulose Biocomposites

JASNA STEVANIC SRNDOVIC

The work has been carried out at INNVENTIA AB

Biopolymer Technology
Department of Chemical and Biological Engineering
CHALMERS UNIVERSITY OF TECHNOLOGY
Göteborg, Sweden 2011

Interactions between Wood Polymers in Wood Cell Walls and Cellulose/Hemicellulose Biocomposites

JASNA STEVANIC SRNDOVIC

ISBN 978-91-7385-517-4

Doktorsavhandlingar vid Chalmers Tekniska Högskola
Ny serie nr 3198
ISSN 0346-718X

Biopolymer Technology
Department of Chemical and Biological Engineering
Chalmers University of Technology
SE-412 96 Göteborg
Sweden
Telephone + 46 (0) 31-772 1000

INNVENTIA AB
Fibre and Material Science
Business area Biorefining
SE-114 86 Stockholm
Sweden
Telephone + 46 (0) 8-676 7000

Cover: Ultrastructure of the primary cell wall of a softwood tracheid.

Chalmers Reproservice
Göteborg, Sweden 2011

To my beautiful children,
Aleksandra and Filip

Interactions between Wood Polymers in Wood Cell Walls and Cellulose/Hemicellulose Biocomposites

JASNA STEVANIC SRNDOVIC
Department of Chemical and Biological Engineering
Chalmers University of Technology
Göteborg, Sweden

INNVENTIA AB
Fibre and Material Science
Business area Biorefining
Stockholm, Sweden

ABSTRACT

A wood fibre is a complex multi component biocomposite that is hierarchically organised. The arrangement of a wood fibre on the ultrastructural level is highly controlled by the interactions between the main structural polymers, i.e. cellulose, various hemicelluloses and lignin, as well as in some parts also pectin and protein. This further determines the mechanical and physical properties of the wood material, and consequently its targeted applications. Despite considerable research in this field during a number of years, the current knowledge on the interactions between the wood polymers is still incomplete and needs improvement. Also, mimicking of natural structures is an inspiration when preparing new materials from renewable resources, hence a comprehensive understanding of the polymer interactions is required.

The first part of this study was to improve the understanding on the molecular interactions within the primary cell wall of spruce wood fibres, and its importance for the energy demand for the refining process during the thermomechanical pulp (TMP) manufacturing. Dynamic FTIR (Fourier transform infrared) spectroscopy in combination with dynamic 2D (two-dimensional) FTIR spectroscopy was used to examine how the lignin, protein, pectin, xyloglucan and cellulose interact in an enriched primary cell wall material. Measurements indicated that strong interactions exist between lignin, protein and pectin, as well as between cellulose, xyloglucan and pectin in this particular layer. Further, by applying a low degree of sulphonation pre-treatment to spruce wood chips, it was shown that the desired ultrastructural changes in the sulphonated primary cell wall material were reached. This selective reaction caused a weakening of the interactions between lignin;pectin, lignin;protein and pectin;protein,

as well as an increased softening and swelling of the material, which were the reasons for the noted energy savings when refining such low sulphonated spruce wood chips.

The second part of this study was to improve the current knowledge on the molecular interaction within the secondary cell wall of a spruce wood fibre, as well as its ultrastructure by studying the orientation of the cellulose, glucomannan, xylan and lignin. Imaging FTIR microscopy was a technique used for studying, which indicated a parallel orientation of polysaccharides with respect to each other and the fibre axis and a partial parallel orientation of lignin. It was suggested that the interactions between the cellulose and glucomannan and the xylan and lignin are dominant but also that interactions between the two hemicelluloses, i.e. glucomannan and xylan, exist.

The third part of this study was to prepare biomimetic biocomposite films, based on cellulose reinforced hemicelluloses. The interactions between these polysaccharides were studied through the prior examined mechanical properties of the biocomposite films using dynamic mechanical analysis (DMA). Here, the understanding of the ultrastructural organisation of the primary and secondary cell walls has been taken as a basis. Intramolecular hydrogen bonding might be created between the cellulose molecules and the unsubstituted areas of the backbone of the hemicellulose molecules, where the lower degree of substitution of xylan results in a more frequent occurrence of intermolecular hydrogen bonding.

This study contributes to an increased understanding between interactions of wood polymers in the primary and secondary cell walls of a softwood tracheid and may serve as a guide for the new generation of biomimetic biocomposites.

***Keywords**: polymer interactions, viscoelasticity, orientation, primary cell wall, secondary cell wall, nanocomposite films, dynamic FTIR spectroscopy, dynamic 2D FTIR spectroscopy, imaging FTIR microscopy, DMA, Norway spruce, wood fibre, cellulose, xyloglucan, xylan, glucomannan, pectin, protein, lignin.*

List of publications

This thesis is based on the work contained in the following papers:

Paper I — Characterizing wood polymers in the primary cell wall of Norway spruce (*Picea abies* (L.) Karst.) using dynamic FT-IR spectroscopy
Jasna S. Stevanic* and Lennart Salmén
2008 *Cellulose* 15(2):285-295

Paper II — The primary cell wall studied by dynamic 2D FT-IR: Interaction among components in Norway spruce (*Picea abies*)
Jasna S. Stevanic* and Lennart Salmén
2006 *Cellulose Chemistry and Technology* 40(9-10), 761-767

Paper III — Interactions among components in the primary cell wall of Norway spruce; How they are affected by different chemimechanical treatments?
Jasna S. Stevanic* and Lennart Salmén
2008 *Journal of Pulp and Paper Science* 34(2):107-112

Paper IV — Orientation of the wood polymers in the cell wall of spruce wood fibres
Jasna S. Stevanic* and Lennart Salmén
2009 *Holzforschung* 63:497-503

Paper V — Bacterial nanocellulose reinforced arabinoxylan films
Jasna S. Stevanic, Catherine Joly, Kirsi S. Mikkonen, Kari Pirkkalainen, Ritva Serimaa, Caroline Rémond, Guillermo Toriz, Paul Gatenholm, Maija Tenkanen, Lennart Salmén*
2011 *Journal of Applied Polymer Science* xxx:xxx-xxx, in press
On-line publication: DOI 10.1002/app.34217

Paper VI — Composite films from spruce galactoglucomannans with microfibrillated spruce wood cellulose
Kirsi S. Mikkonen*, Jasna S. Stevanic, Catherine Joly, Patrice Dole, Kari Pirkkalainen, Ritva Serimaa, Lennart Salmén, Maija Tenkanen
2011 *Cellulose* xx:xxx-xxx, in press
On-line publication: DOI 10.1007/s10570-011-9524-0

Contribution report

Paper I — Main author. Took an active part in planning the experiments and performed most of the experimental work.

Paper II — Main author. Took an active part in planning the experiments and performed most of the experimental work.

Paper III — Main author. Took an active part in planning the experiments and performed most of the experimental work.

Paper IV — Main author. Took an active part in planning the experiments and performed most of the experimental work.

Paper V — Co author. Took an active part in planning the experiments and performed most of the experimental work regarding the preparation of films, tensile and mechanical testing using DMA.

Paper VI — Co author. Took an active part in planning the experiments and performed most of the experimental work regarding the preparation of films, tensile and mechanical testing using DMA.

Other relevant publications

Analysis of thermally treated wood samples using dynamic FT-IR-spectroscopy
Lennart Salmén*, Hans Possler, Jasna S. Stevanic and Stefanie E. Stanzl-Tschegg
2008 *Holzforschung* 62:676–678

Localisation and characterisation of incipient brown-rot decay within spruce wood cell walls using FT-IR imaging microscopy
Karin Fackler*, Jasna S. Stevanic, Thomas Ters, Barbara Hinterstoisser, Manfred Schwanninger, Lennart Salmén
2010 *Enzyme and Microbial Technology* 47:257-267

FT-IR imaging microscopy to localise and characterise simultaneous and selective white-rot decay within spruce wood cells
Karin Fackler*, Jasna S. Stevanic, Thomas Ters, Barbara Hinterstoisser, Manfred Schwanninger, Lennart Salmén
2011 *Holzforschung* 65:xxx-xxx, in press
On-line publication: DOI 10.1515/HF.2011.048

Cell wall polymers orientation in fibres from branches of hardwood and softwood – a polarized FTIR study
Jasna Simonović, Jasna S. Stevanic, Daniela Djikanović, Lennart Salmén*, Ksenija Radotić*
Submitted to Macromolecular bioscience

Structural organisation of the wood polymers in the wood fibre structure
Lennart Salmén*, Anne-Mari Olsson, Jasna S. Stevanic, Jasna Simonović, Ksenija Radotić
2011 *Proceedings of the 16th ISWFPC*, Tianjin pp.xxx-xxx, in press

Abbreviations

AGX	arabinoglucuronoxylan
AX	arabinoxylan
BC	bacterial cellulose
CTMP	chemithermomechanical pulp
DMA	dynamical mechanical analysis
DP	degree of polymerisation
2D FTIR	two dimensional Fourier transform infrared
σ_B	stress at break
E	Young's modulus
E'	storage modulus
ε_B	strain at break
FTIR	Fourier transform infrared
GGM	galactoglucomannan
gly	glycerol
H	holocellulose fibre with exposed S_2 cell wall
LCC	lignin-carbohydrate complex
MFC	microfibrillated cellulose
NMR	nuclear magnetic resonance
P	primary cell wall
rAX	rye arabinoxylan
rDAX	rye debranched arabinoxylan
RH	relative humidity
S	secondary cell wall
S_1	outer secondary cell wall
S_2	middle secondary cell wall
S_3	inner secondary cell wall
SEM	scanning electron microscopy
$\tan\delta$	loss tangent
T_g	glass transition temperature
TMP	thermomechanical pulp
W	spruce wood fibre with exposed S_2 cell wall
XyG	xyloglucan

Table of contents

1 INTRODUCTION

1.1 Background

The interactions between the structural polymers, i.e. cellulose, hemicelluloses and lignin but also, in some parts, pectin and protein, determine the ultrastructural organisation in a wood fibre. This further determines the mechanical and physical properties of wood, and consequently its targeted applicational possibilities. The understanding on the interactions of the wood polymers is still incomplete and needs improvement.

Mechanical pulping is a highly energy demanding process. One of the major tasks for the pulp and paper making industries today has been to focus on energy saving. The fibre separation process determines the amount of energy required in the refining process. The chemical and physical properties of the outer fibre wall layers differ from those of the inner fibre wall layers. The presence of strong interactions among polymers and, especially, the relatively high content of pectin and protein in the primary cell wall mean that there is a very good possibility of selectively attacking the polymers in the primary cell wall [1,2]. By selectively attacking the primary cell wall using different chemical and/or enzymatic treatments [3-6], pulp with good properties can be produced. Changing fibre properties by utilising such treatments, if they are controlled properly, is also a means of significantly reducing energy consumption in the refining process [7,8]. For a good fibre separation, it is however necessary to have an appropriate surface fibrillation or roughness in the fibre rupture zone. A softening of pectin at a relatively low moisture level, or an addition of protease that attacks protein in the primary cell wall could make the primary cell wall quite compliant for such a surface fibrillation, a necessity in order to be able to develop the fibre in the subsequent refining process [1]. Improved knowledge of the primary fibre wall is thus of essential importance for attaining a more efficient refining process in mechanical pulping as well as for producing a high quality mechanical pulp. Dynamic Fourier transform infrared (FTIR) spectroscopy, in combination with dynamic 2D (two-dimensional) FTIR spectroscopy, is a technique suitable for studying complex polymeric materials. This technique offers an opportunity of analysing the molecular interactions as well as the viscoelastic behaviour of polymeric materials [9], why the technique here used.

The secondary cell wall of a wood fibre, especially its most dominant layer, the S_2 layer, making up to 85% of the total thickness of the cell wall [10], plays an essential role regarding the mechanical and physical properties of a whole fibre. The secondary cell wall is composed of three different layers; the S_1, S_2 and S_3 layers. The constitutive components in the softwood, such as spruce, are the polymers: cellulose, hemicelluloses (i.e. *O*-acetylgalactoglucomannan, arabino-4-*O*-methylglucuronoxylan) and lignin. The organisation of the secondary cell wall is highly complex and the knowledge of it on the ultrastructural level still needs to be improved. The majority of the studies, in this respect, have been concentrated on investigation of the cellulose microfibrils, while other constituents, which also play an important role, especially for properties in transverse direction, have been less investigated. Their orientations, interactions and ultrastructural organisation are still unclear. The orientation of the hemicelluloses and lignin, which are amorphous polymers, may, particularly under moist conditions, play a dominant role for the mechanical properties [11]. Imaging FTIR microscopy is a technique appropriate for studying the orientations and interactions of the polymers in various samples on a microscale, and therefore here adopted.

In general, today's food packaging materials are based on fossil resources, hence a global warming issue due to the coupling to an increasing emission of CO_2 in nature. An increasing concern for the maintenance of the environment, but also for sustainability of resources is required. On these bases, consumers can have positive view on environmentally friendly, biodegradable and sustainable package materials, based on renewable polymers. Nature has for a long time developed structures having astonishing properties suitable to resist different internal and external stresses. These varying hierarchical structures in nature can be inspiring for better understanding of possible design approaches of new biocomposite materials in order to accomplish proper performance for targeted applications. Films made of plant-derived non-food polysaccharides, such as various hemicelluloses and celluloses, may provide a potential alternative to the oil-based materials. The physical properties of hemicellulose-based films are though a challenging issue due to its influence by the environmental conditions of temperature and humidity on the properties. Hemicelluloses are hydrophilic and as such show good barrier properties against oils and fats, but they are not efficient as moisture and water vapour barriers [12]. However,

they tend to make a dense network providing good oxygen barrier properties [13-15]. Their mechanical, i.e. viscoelastic, properties can be questioned for packaging purposes, and one probable solution to improve the performance of hemicelluloses films is reinforcement of cellulose. Improved knowledge of the mechanical properties is here of essential importance. Dynamic mechanical analysis (DMA) is a powerful tool for studying the viscoelastic behaviour of polymeric materials and of molecular interactions, and thus utilised for these studies.

1.2 Aim of the study

The aim of this study was to investigate the interactions between wood polymers in various materials: i.e. (a) the primary cell wall and (b) the secondary cell wall of spruce tracheids, and for (c) cellulose/hemicellulose biocomposite films. Measuring techniques, primarily based on mechanical spectroscopy and IR spectroscopy as well as the combination of these techniques, were adopted to examine these interactions.

(a) The first objective was to determine the interactions among the polymers in the primary cell wall of spruce wood fibres and its ultrastructural organisation, in order to better understand ways of attacking this layer for a more energy efficient defibration process. Moreover, an additional objective was to gain more knowledge when it came to the effect of a low degree of sulphonation on the changes in the molecular interactions and the ultrastructure of the primary cell wall. The primary technique adopted was dynamic FTIR spectroscopy.

(b) The second objective was to determine the orientations and interactions of the polymers in the secondary cell wall of spruce wood fibres, in order to better understand its ultrastructural organisation for enhancing fibre properties. The primary technique utilised was imaging FTIR microscopy.

(c) The third objective of this work was to determine mechanical properties of nanocellulose reinforced hemicellulose films and the interactions of the constitutive polymers. Here, an improved knowledge about the ultrastructural organisation of the secondary cell wall as well as the ultrastructural organisation of the primary cell wall was used as background information. The primary technique utilised was DMA.

2 STRUCTURAL BIOPOLYMERS

The principal biopolymers in wood fibres are cellulose, hemicelluloses and lignin. Pectin, protein, extractives and some inorganic compounds are also present in wood fibres, but only as minor compounds. A wood fibre is built up by a number of different cell wall layers, such as the primary cell wall and the secondary cell wall. To some extent, the composition of the primary cell wall, being the remains of the living cell, differs from the composition of the secondary cell wall. In contrast to the secondary cell wall, the primary cell wall of softwood contains pectin and protein with the most abundant hemicelluloses in it being xyloglucans (XyGs). Galactoglucomannans (GGMs) and arabinoglucuronoxylans (AGXs), the major hemicelluloses in the secondary cell wall of softwood, also occur as minor components of the primary cell wall of softwood.

Hemicelluloses similar to those in wood, i.e. arabinoglucuronoxylans (AGXs), may also be obtained from cereal grains. In for instance rye, the main hemicelluloses are arabinoxylans (AXs) and minor hemicelluloses are β-glucans, i.e. β-1,3/1,4-D-glucans.

2.1 Cellulose (β-1,4-D-glucan)

Cellulose is the most abundant organic material on Earth and principal reinforcing component of all plant cell walls. Cellulose accounts for about 40% to 50% by weight of the wood fibre, and is mostly located in the secondary cell wall (~50%) but also in the primary cell wall (~20%). Cellulose is a linear homopolysaccharide, composed of β-D-glucopyranose units (β-D-Glc*p*), linked together by covalent β-1,4-glycosidic bonds. Repeating unit in a cellulose chain is a disaccharide unit, i.e. cellobiose, built of two β-D-Glc*p* units, which are oriented 180° in relation to each other (Figure 1). The β-D-Glc*p* units have a chair conformation in cellulose molecules and their degree of polymerisation (DP, i.e. number of glucose residues in a chain) is about 10,000 in wood [16]. The native cellulose, cellulose I, is built up of two crystalline allomorphs, Iα and Iβ, as demonstrated by CP-MAS ^{13}C-NMR techniques [17]. The two allomorphs differ with respect to their crystal packing, hydrogen bonding and molecular conformation. Examinations using X-ray and electron diffraction techniques shows

that cellulose Iα has a one-chain triclinic unit cell, while cellulose Iβ has a two-chain monoclinic unit cell [18,19].

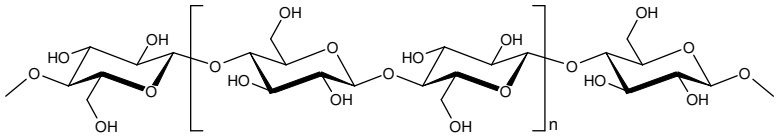

***Figure 1**: Structure of cellulose and a cellobiose residue (length 1.03 nm) with the β-1,4-glycosidic bond. The β-D-glucopyranose (β-D-Glc**p**) units are in a chair conformation. They are at an angle of 180˚ in relation to each other.*

The cellulose molecules arrange themselves in longitudinal strands, i.e. microfibrils, that are composed of several crystalline regions (60 nm in length) interrupted by noncrystalline or paracrystalline areas along its length [20]. The width, length, crystallinity and DP of cellulose differ, depending on the source and the age of the tissue. The DP of the primary cell wall cellulose is about 2,000-6,000 and quite polydisperse, while the DP of the secondary cell wall cellulose is about 14,000 and more homogeneous [21]. The cellulose molecules have a strong tendency to form intermolecular and intramolecular hydrogen bonds. Two intramolecular hydrogen bonds, i.e. O2'-H…O6 and O3-H…O5', and one intermolecular hydrogen bond, i.e. O6-H…O3, exist [22]. This parallel hydrogen bonded structure of the chain cellulose molecules form what is called *microfibrils*, despite their nanoscale dimensions. The size of softwood microfibrils is about 3.5 nm [23,24]. The bundle aggregations of the microfibrils are referred to as *microfibril aggregates*. They have variable dimensions in the cell wall of wood, with an average size of between 10 nm and 30 nm [25,26]. This structure of the cellulose is responsible for the longitudinal tensile strength of wood fibres.

2.2 Hemicelluloses

Hemicelluloses are heteropolysaccharides, with a DP of around 100 in softwoods and 200 in hardwoods. They are present in both the primary and the secondary cell walls, and in a small amount also the middle lamella region. Hemicelluloses are also major constituents of cereal cell walls. Hemicelluloses are a large group of branched heteropolymers, composed of several different monomer units in the form of pyranose and furanose rings (see Figure 2), such as: (a) β-D-glucopyranose (β-D-Glc*p*),

(b) α-D-xylopyranose (α-D-Xyl*p*), (c) β-D-xylopyranose (β-D-Xyl*p*), (d) β-D-mannopyranose (β-D-Man*p*), (e) α-D-galactopyranose (α-D-Gal*p*), (f) β-D-galactopyranose (β-D-Gal*p*), (g) α-L-rhamnopyranose (α-L-Rha*p*), (h) α-L-arabinofuranose (α-L-Ara*f*) and (i) β-L-arabinofuranose (β-L-Ara*f*). Some sugar acids, such as: (j) α-D-glucopyranuronic acid (α-D-Glc*p*A), (k) 4-*O*-methyl-α-D-glucopyranuronic acid (4-*O*-Me-α-D-Glc*p*A) and (l) α-D-galactopyranuronic acid (α-D-Gal*p*A), are very important compounds in some hemicelluloses. These monomers occur in different proportions in the hemicelluloses.

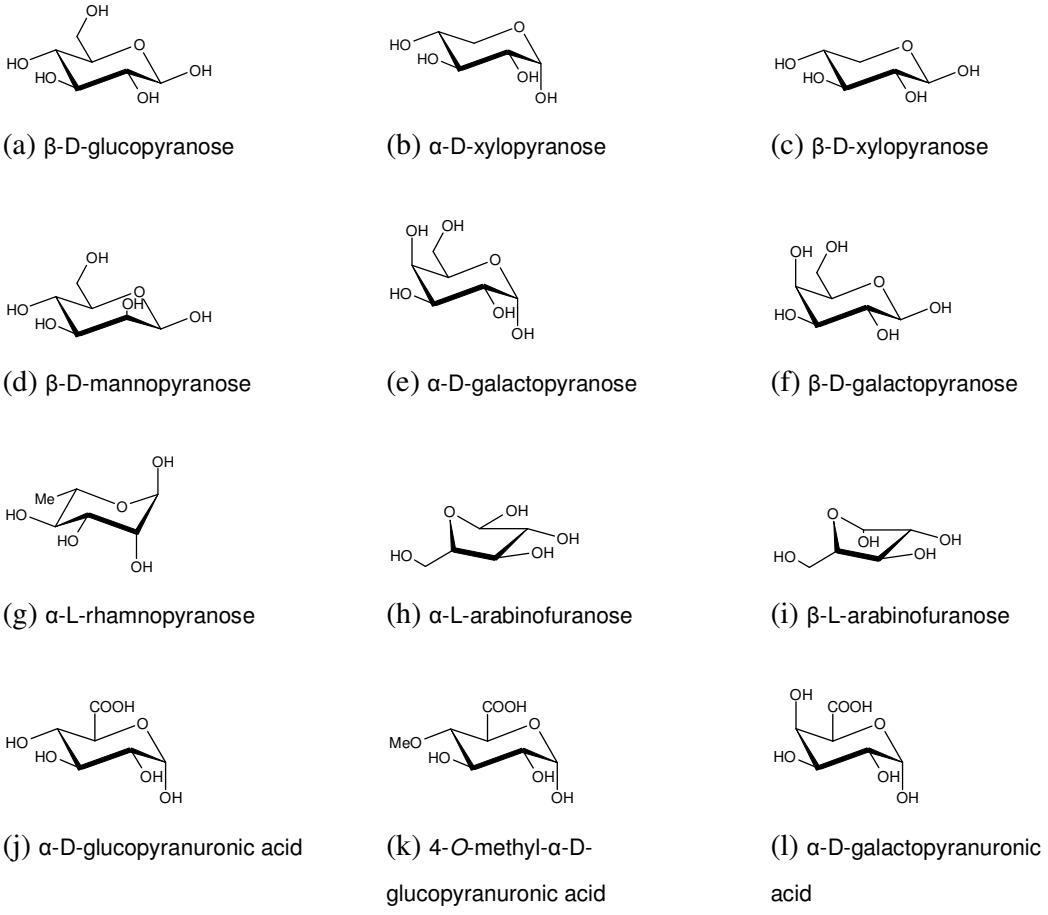

***Figure 2**: Structure of some monosaccharides and sugar acids.*

The most common hemicelluloses in softwoods are (1) in the primary cell wall – xyloglucans (XyGs) and small amount of galactoglucomannans (GGMs) and arabinoglucuronoxylans (AGXs), and (2) in the secondary cell wall – galactoglucomannans (GGMs) and arabinoglucuronoxylans (AGXs). The most common hemicelluloses in cereal cell walls are arabinoxylans (AXs) and β-glucans.

The hemicelluloses are amorphous polymers, without a tendency to form crystalline regions in their native form in the cell walls. The purpose of the hemicelluloses is to serve as binders in the cell walls providing for its flexibility, but they are also essential for the formation of the cellulose microfibril structure during the deposition of the cellulose in the cell wall [27,28].

2.2.1 Xyloglucans (XyGs)

Xyloglucans are major hemicelluloses in the softwood primary cell wall (20% of the dry weight of the cell wall), but also in the hardwood primary cell wall. They have a backbone composed of β-1,4-linked β-D-Glc*p* residues, which are substituted at *O*-6 by α-D-Xyl*p* residues. A series of Glc_4Xyl_3 repeating units have been reported [29] (see Figure 3). Some α-D-Xyl*p* residues can be extended by the substitution, at *O*-2, with α-L-Ara*f*, β-D-Gal*p* and α-L-Fuc*p*-1,2-β-D-Gal*p* residues. Xyloglucans are partly acetylated in their native state [30]. Some or most of the xyloglucans are hydrogen bonded to cellulose and covalently bonded to pectin [21]. Xyloglucans have a structural role in the primary cell walls and together with cellulose form a load-bearing network that prevents cells from rupturing under mechanical stress [28].

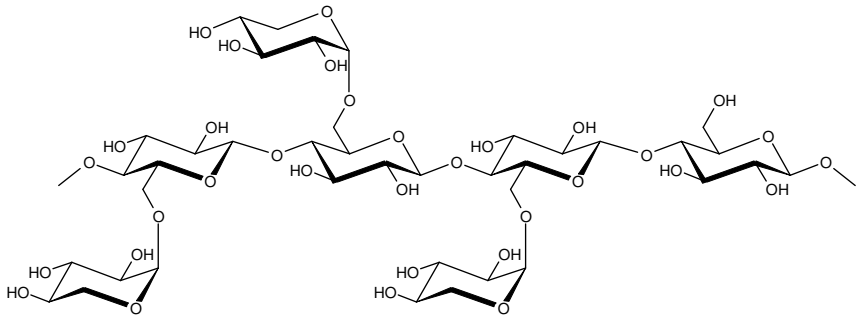

***Figure 3**: Structure of xyloglucan.*

2.2.2 Galactoglucomannans (GGMs)

Galactoglucomannans (*O*-acetylgalactoglucomannans) are the main hemicelluloses of the softwood secondary cell wall (approximately 20%) built up by β-1,4-linked β-D-Glc*p* and β-D-Man*p* units (see Figure 4). They are partly acetylated, at *O*-2 and *O*-3, linear and slightly branched polysaccharides with α-D-Gal*p* units substituted to β-D-Man*p* residues at *O*-6. The galactoglucomannans are divided into two fractions, depending on the different distribution of α-D-Gal*p* substituents having a galactose:glucose:mannose ratio of approximately 1:1:3 in the high-galactose fraction,

and 0.1:1:4 in the low-galactose fraction, but the ratio varies for the different tissues [21,31,32]. In the hardwood secondary cell wall, a small amount (3% to 5%) of *O*-acetylglucomannans is present, with a structure similar to the structure of the backbone of galactoglucomannans. They are also acetylated at *O*-2 and *O*-3 positions of some of mannose units and a glucose:mannose ratio is approximately 1:2 [21,33].

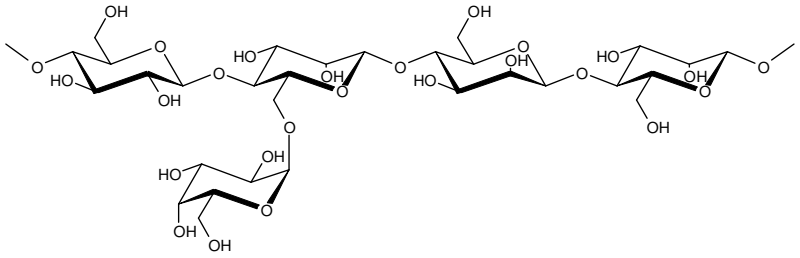

***Figure 4**: Structure of galactoglucomannan.*

2.2.3 Xylans (β-1,4-D-xylans)

Xylans make a group of branched linear polysaccharides that can be found in many woody plants, such as softwoods (mainly in secondary cell walls), and in almost all annual plants, such as grasses (in primary cell walls).[34,35] Cereal primary cell walls, such as from wheat, barley, oat and rye, are rich in xylans.[21] The chemical structure of xylans varies significantly depending on their source. The backbone of xylans is built up of β-1,4-linked β-D-Xyl*p* units, which are further substituted with varying degrees by α-L-Ara*f* groups. Other substituents found in xylans are α-D-Glc*p*A (or its 4-*O*-methyl ether, 4-*O*-Me-α-D-Glc*p*A), β-D-Xyl*p*, acetyl and feruloyl groups [21,31]. A disaccharide side chain, i.e. β-D-Xyl*p*-α-L-Ara*f*, are also present [36]. The degree of substitution of xylans determines their ability to dissolve in water and their ability to bind to cellulose. Xylans with a lower degree of substitution are less water soluble and bind tightly to cellulose, while xylans with a high degree of substitution are more water soluble and bind less tightly to cellulose by preventing intermolecular hydrogen bonding [21,31].

2.2.3.1 Arabinoglucuronoxylans (AGXs)

The softwood secondary cell wall contains about 5% to 10% arabinoglucuronoxylans (arabino-4-*O*-methylglucuronoxylans). These polysaccharides are formed by β-1,4-linked β-D-Xyl*p* units, partly substituted at *O*-2 by single 4-*O*-Me-α-D-Glc*p*A residues (having a xylose:glucuronic acid ratio of 5:1), and additionally substituted at

O-3 by single α-L-Ara*f* residues (a xylose:arabinose ratio 10:1.3) (Figure 5) [21,29,31,32]. In the hardwood secondary cell wall, the main hemicelluloses (15% to 30%) are *O*-acetil-4-*O*-methylglucuronoxylans, which are in contrast to arabinoglucuronoxylans acetylated, at *O*-2 and *O*-3. Structurally these two homocelluloses are similar with an exception where, in fact, the acetylation in hardwood glucuronoxylans replaces the arabinose units in softwood arabinoglucuronoxylans [21]. Glucuronoxylans have a xylose:glucuronic acid ratio of 10:1 [29].

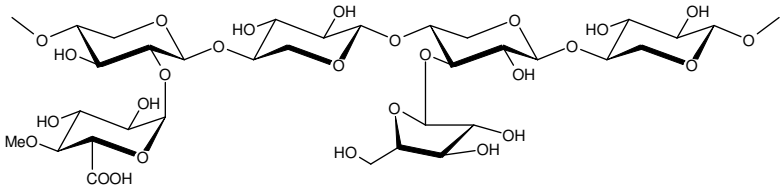

***Figure 5**: Structure of arabinoglucuronoxylan.*

2.2.3.2 Arabinoxylans (AXs)

Arabinoxylans are mostly abundant in the cell walls that surround the cells in the starchy endosperm, and the aleurone layer (about 60%-70%) of the cereal grain [37]. The total amount of arabinoxylans in rye (*Secale cereale* L.) grain is reported to 7%-12% [38,39]. The backbone of these polysaccharides are formed by β-1,4-linked β-D-Xyl*p* units. In arabinoxylans from rye starchy endosperm cell walls, the β-D-Xyl*p* units are both mono- and di-substituted at *O*-2 and *O*-3 positions by α-L-Ara*f* units (Figure 6). The average arabinose:xylose (or Ara/Xyl) ratio in rye water soluble arabinoxylans is about 1:2 to 1:1, where the mono-substitution dominates over the di-substitution in the structure [14,34,40].

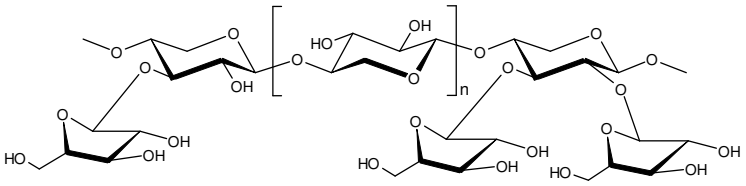

***Figure 6**: Chemical structure of rye arabinoxylan, n ≥ 1.*

2.3 Pectins

Pectins are very hydrophilic and very complex structural polysaccharides. They are actually composed of networks of polymers and are present in the primary cell walls

of the tracheids, the ray cell walls, pit membranes and the middle lamella [41]. The primary cell wall of developing softwood xylem consists of more than 30% pectin [42]. Pectic polysaccharides can be divided into different groups: (1) galacturonans (homogalacturonan (HGA), rhamnogalagturonan I (RG-I), rhamnogalagturonan II (RG-II) and xylogalacturonan (XGA)), (2) arabinans, (3) galactans and (4) arabinogalactans (arabinogalactan I (AG-I) and arabinogalactan II (AG-II)) [31]. The most characteristic glycosyl residue in the pectic polysaccharides is the galacturonosyl residue, but rhamnosyl, arabinosyl and galactosyl residues are also present. The galacturonans are grouped in a family of acidic polysaccharides. Arabinans, galactans and arabinogalactans are otherwise grouped in a family of neutral polysaccharides. The neutral polysaccharides are most likely covalently attached to the backbone of rhamnogalacturonans as side chains (at *O*-4 of the 1,2-linked rhamnopyranosyl residues) [21]. Pectic polysaccharides may be covalently linked to protein and lignin. [31]

The backbones of the homogalacturonan (HGA), the rhamnogalagturonan II (RG-II) and the xylogalacturonan (XGA) consist of α-1,4-linked α-D-Gal*p*A (see Figure 7). The HGA (with a DP of about 70) is a homopolymer, whose α-D-Gal*p*A residues are partly acetylated at *O*-3 and partly methyl-esterified at *O*-6 (i.e. on carboxylic acid group). The distribution of the methyl-esterified units is not completely known. The HGA is covalently linked to the RG-I and the RG-II, while the XGA is connected covalently to the RG-I in the cell wall. Boron (B) is known to selectively bind to RG-II in pectin and form a cross-link [21,28,31].

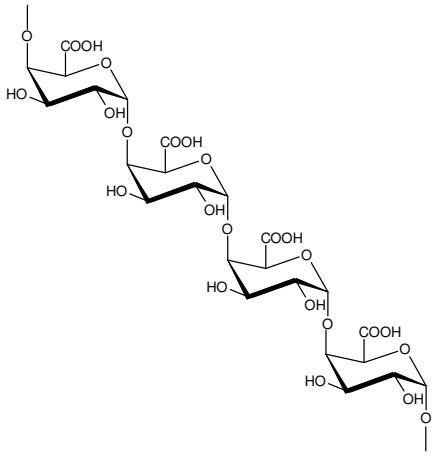

***Figure 7**: Structure of homogalacturonan (HG).*

Rhamnogalagturonan I (RG-I) has another configuration in its backbone (see Figure 8). It is composed of the repeating disaccharide units, [1,2-α-L-Rha*p*-1,4-α-D-Gal*p*A-1,2]$_n$, where *n* can be greater than 100 [43]. Rhamnogalacturonans are branched polymers, with various linked side chains, attached to *O*-4 of α-L-Rha*p* units. The α-D-Gal*p*A units of the RG-I are acetylated, on *O*-2 and *O*-3. The monosaccharides, such as β-D-Gal*p*, α-L-Ara*f* or α-L-Fuc*p* are major compounds in these side chains. The α-L-Rha*p* units are much more abundant in the RG-I than in the RG-II, for example, and they are only present in the side chains of the RG-II. The RG-II side chains are further specified by presence of 2-*O*-Me-α-L-Fuc*p*, 2-*O*-Me-α-D-Xyl*p*, apiose, aceric acid and KDO (3-deoximan-nonctulosonic acid) [21,28,31].

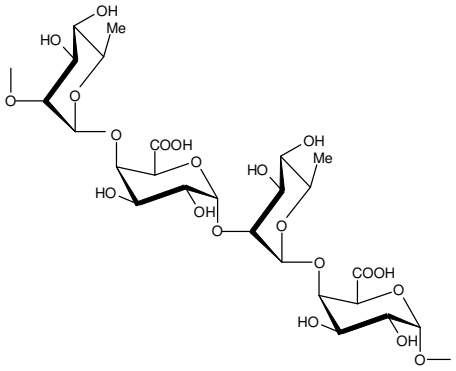

***Figure 8**: Structure of backbone of rhamnogalacturonan I (RG-I).*

Xylogalacturonan (XGA) is a branched polymer, with a side chain formed by β-D-Xyl*p* units and β-1,3-linked on the galacturonan backbone (see Figure 9). This polysaccharide or, more precisely, the α-D-Gal*p*A units can also be methyl-esterified, as in the HGA [21,28,31].

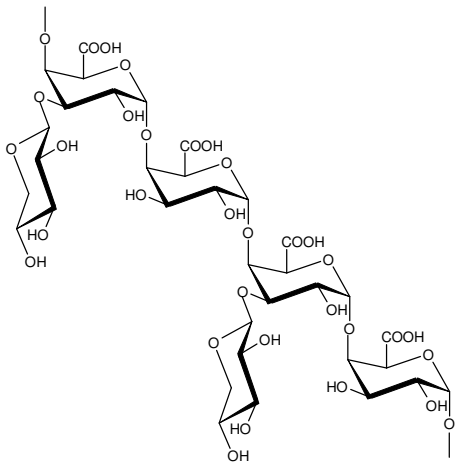

***Figure 9**: Structure of xylogalacturonan (XGA).*

Arabinogalactans (AG) are branched polysaccharides. The AG-I has a backbone formed of β-1,4-linked β-D-Gal*p* units and α-1,5-linked α-L-Ara*f* short side chains that are substituted at *O*-3 (see Figure 10). The AG-II is a highly branched polysaccharide that contains β-3-, β-6- and β-3,6-linked β-D-Gal*p* residues, including various amounts of α-L-Ara*f*, β-D-Gal*p*A and β-D-Glc*p*A residues. It seems that AG-II and AG proteins (AGPs) are not components of the primary cell wall. They are located instead in the periplasmic space. AGPs are a family of the hydroxyproline (*Hyp*)-rich glycoproteins [21,28,31].

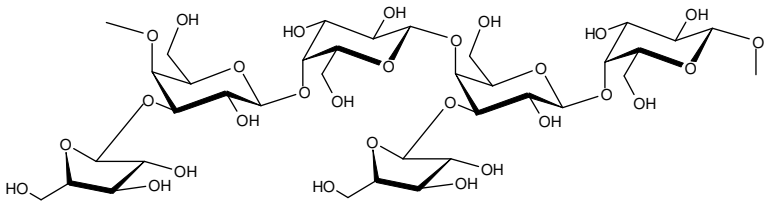

***Figure 10**: Structure of arabinogalactan I (AG-I).*

The total amount of pectin in wood is low, however it exists as high local concentrations, e.g. in the compound middle lamella, the ray cell walls and the pit membranes. As with most pectins, the galacturonans are reported in two forms, viz. as methyl-esterified and unesterified (or low esterified). The pectin that is mainly abundant is in a methylated form, as shown in immunolocalisation studies, using monoclonal antibodies JIM5 and JIM7, by Hafrén et al [44]. Methyl-esterified galacturonan is mostly present in lignified tissues. The unlignified tissues mainly contain unesterified pectins i.e. acetic galacturonan. The methyl-esterified and unesterified pectins are distributed more in the radial than in the tangential middle lamella of spruce sapwood. It seems that the lignification process results in an increase in the methyl-esterified pectin and a decrease in the acidic pectin [44,45]. Unesterified pectins or acidic galacturonan usually form gels. The nature of this phenomenon is explained by the affinity of negatively charged carboxylic groups from homogalacturonan that form complexes with cations, mostly calcium (Ca^{2+}) – calcium-gels. The complexes that are formed are termed “egg box” structures [21,46].

2.4 Proteins

The primary cell wall and pit membranes contain up to 10% proteins. The most well-known structural proteins of a cell wall are extensins, which are a class of hydroxyproline (*Hyp*)-rich glycoproteins (HRGPs). The AGPs are also a class of hydroxyproline (*Hyp*)-rich glycoproteins. In the walls of xylem elements, there are also other proteins identified, such as the proline (*Pro*)-rich proteins (PRPs), the glycine (*Gly*)-rich proteins (GRPs) [21] and the proline, threonine and glycine (*Pro-Thr-Gly*)-rich proteins (PTGRPs). The PRPs and PTGRPs have been found in lignified cell walls. Several studies show that lignin can make covalent cross-links with proteins and pectins and, as a result, provide mechanical support in the cell wall [47].

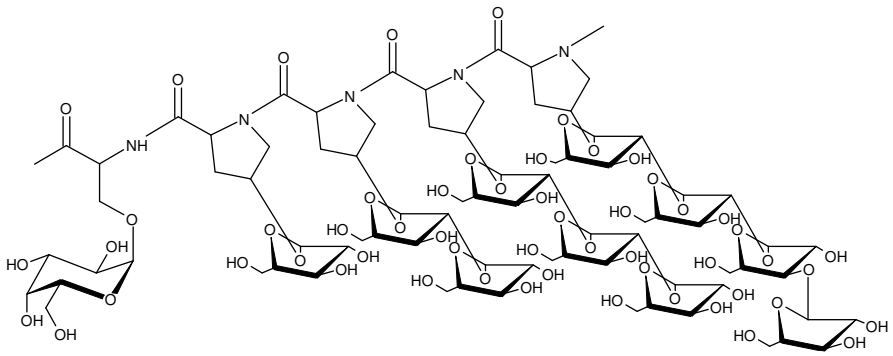

***Figure 11**: Structure of the glycosilated region of the hydroxyproline-rich glycoprotein, extensin.*

Extensins are characterised through a peptide portion, which is *O*-glycosilated by a carbohydrate portion. The peptide portion of the extensins is built up of the following amino acid residues: hydroxyproline (*Hyp*), serine (*Ser*), proline (*Pro*), tyrosine (*Tyr*), lysine (*Lys*), threonine (*Thr*) and valine (*Val*). These residues usually form numerous repeat sequences in the protein macromolecules, viz. pentapeptides – Ser-$(Hyp)_4$, Ser-$(Pro)_4$, tetrapeptide – $(Tyr\text{-}Lys)_2$ and tripeptide – (Thr-Pro-Val). The carbohydrate portion of the extensins can contain the arabinose side chains with mono-, di- or tri-β-L-Ara*f* units β-1,2-linked, and the tetra- units arabinose side chain where tri β-L-Ara*f* units are β-1,2-linked and one α-L-Ara*f* unit is α-1,3-linked). The arabinose side chains are 1,4-linked to the Hyp residues, and the single α-D-Gal*p* unit is 1,2-linked to the Ser residue (see Figure 11). Proteins make intramolecular cross-links, protein-protein or protein-phenolic-protein (isodithyrosine) links, as well as covalent cross-links between extensin and RG-I [48].

2.5 Lignin

Lignin is highly abundant biopolymer on Earth and it makes up 20% to 30% of wood by weight. Lignin is a large family of aromatic branched polymers, built up of hydroxyphenyl propane units, in a three-dimensional (3D) structure. It is less hydrophilic than carbohydrates. Lignin is present in the middle lamella as the most abundant polymer, it also exists in the primary cell wall, but the largest quantity is found in the secondary cell wall. Lignin is deposited successively through the cell walls. It is started to deposit, toward the end of primary cell wall growth after finished cell expansion and after that the S_1 layer started to form, in the middle lamella and at the cell corners of the primary cell wall. Further, it is continued to deposit in the primary cell wall and in the S_1 layer during the S_2 layer formation. And finally, it is the most active deposited through the secondary cell wall after that the S_3 layer finished to form. The main compounds of native lignin are the monolignols: p-coumaryl alcohol, coniferyl alcohol and sinapyl alcohol (see Figure 12).

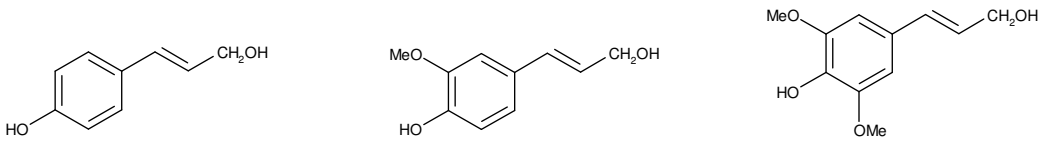

(a) p-coumaryl alcohol (b) coniferyl alcohol (c) sinapyl alcohol

***Figure 12**: Structures of monolignols*

Lignin in softwood is mainly composed of the coniferyl alcohol units, while lignin in hardwood is built as a co-polymer from both the coniferyl and sinapyl alcohol units. However, large modifications of the lignin chemical structure exist depending on the plant species, tissue, as well as different layers in the cell wall. It consists of a variety of intramolecular bonds. The most present bonds forming the 3D network in softwood lignin are: β-*O*-4 (59%), β-5 (17%), β-β (10%), 5-5 (9%) and β-1 (7%) [49]. Lignin is incorporated in complex structure of the cell walls by covalent linking to hemicelluloses, i.e. (1) the α–benzyl hydroxyl residue of lignin is linked by ether bonds to the D-Man*p*, D-Gal*p* and D-Glc*p* residues at *O*-6 and to the D-Xyl*p* residues at *O*-2 and *O*-3, (2) the α–benzyl hydroxyl residue of lignin is linked by ester bonds to the carboxyl group of the D-Glc*p*A residue, and also (3) glycosidic bond and (4) acetal bond are possible [50]. Lignin acts in the cell wall, among other functions, as

providing for the compression strength of a fibre as well as providing the hydrophobic surface of a fibre needed for the transport of water [10].

3 STRUCTURE OF THE WOOD FIBRE

Wood, i.e. the xylem, in the stem of a tree is composed of different wood cells. The most important wood cells are longitudinal tracheids in softwoods (*Conifers - Gymnosperms*) (about 95%), and libriform fibres in hardwoods (*Dicot Angiosperms*). These cells are often referred to as fibres. Apart from fibres, there is an abundance of ray cells in softwoods (important for transport and storage of water and organic nutrients), while ray cells and vessel cells exist in hardwoods. Pits are also present in both of the wood categories. They are passages for water between two neighbouring cells. Softwood mostly consists of fibres that are structured in annual rings, where one ring consists of both earlywood tracheids mainly involved in transport of water and dissolved minerals, and latewood tracheids having a mechanical supporting function. Earlywood tracheids are formed in the spring and summer. They have thinner walls and a larger lumen than the latewood tracheids, which are formed at the end of the growing season. The fibre cell wall is composed of two phases, a fibrillar phase and a matrix phase. The fibrillar phase serves as a kind of reinforcement and is composed of cellulose microfibrils, while the matrix phase consists of hemicelluloses, lignin, and in the case of the primary cell wall of small amounts of pectin and protein. The fibre cell wall is further built up by an assembly of concentric layers, which differ in their structure as well as in their chemical composition. The cell wall layers are mostly characterised by the angular orientation of the microfibrils, i.e. the crystalline cellulose regions, with respect to the longitudinal cell axes, i.e. by the right direction (Z-helix) and the left direction (S-helix) of the microfibrils. The layers are clearly visible in an electron microscope [26]. This is schematically shown in Figure 13. The cell is surrounded by a middle lamella (ML), which acts as a gluing medium holding the cells together. The middle lamella has varying thicknesses, especially at the cell corners, between 0.5 µm and 1.5 µm. The main substances in the middle lamella are pectin, at an early stage of growth, and lignin, at a later stage of growth. The primary cell wall (P) is a thin layer (0.1 µm) composed of cellulose, hemicelluloses, pectin, protein and lignin. The secondary cell wall (S) is formed during the thickening of a cell wall, where cellulose, hemicelluloses and lignin are major building components. It is divided into three layers, viz. the thin outer layer (S_1) (0.1 µm to 0.35 µm), the thick middle layer (S_2) (1 µm to 10 µm) and the thin inner layer (S_3) (0.5 µm to 1.1 µm) [10]. The thin S_1 and S_3 layers are rich in hemicelluloses, while the thick S_2 layer is

rich in cellulose. The outer layer (S_1) is closest to the primary cell wall. Its microfibril angle is between 60˚ and 80˚ (in a clockwise direction, S-helix). The middle layer (S_2) forms the larger portion of the cell wall, having a microfibril angle (in a counterclockwise direction, Z-helix), which vary between 10° and 30˚, in earlywood, and between 0° and 10˚, in latewood. The inner layer (S_3), adjacent to the cell lumen (L), contains microfibrils in an S-helix, with an angle between 60° and 90˚. The microfibrils in the S_3 layer are oriented almost perpendicular to the microfibrils in the S_2 layer [10,51]. The warty layer (W) is a thin amorphous membrane, located on the outside of the S_3 layer, i.e. towards the cell lumen. All softwoods have this segment in their cell wall, however not all hardwoods do.

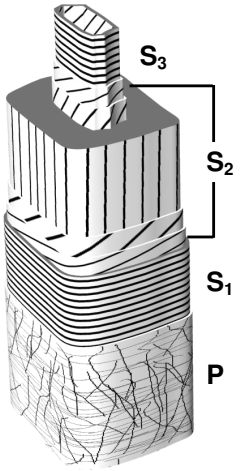

***Figure 13**: Structure of a fibre cell wall, as illustrated by Brändström [52]. P – primary cell wall, S_1 – outer secondary cell wall, S_2 – middle secondary cell wall and S_3 – inner secondary cell wall.*

3.1 The primary cell wall

The primary cell wall is an essential unit of all cells that is formed at the beginning of the cell development. For gymnosperm tracheids, the development starts by *a tangential division* of a mother cambial cell into two daughter cells, and form the cell plates, which mostly consist of a hard pectin gel cross-linked with Ca^{2+} ions. The two cells that will conduct water further undergo a period of *a radial expansion*. The cells formed at this stage have reached their final size, and they are composed of a primary cell wall only, and consist of cellulose microfibrils and hemicelluloses cross-linked by Ca^{2+} ions between hemicelluloses and by hydrogen bounds between cellulose

microfibrils and hemicelluloses [10]. The primary cell wall must yield to allow its own growth and it is involved into intensive biosynthesis and rearrangement of the cell wall components. The cellulose microfibrils, (synthesised at the plasma membrane by so-called terminal rosette complexes (TCs), suggested to be cellulose-synthesising enzyme complexes [53]), are formed as a multilayered irregular network in the outer side of the primary cell wall. The inner side of the primary cell wall contains microfibrils that are more perpendicularly oriented to the cell axis [16]. Relatively large distances are present among the microfibrils in the thin primary cell wall, which results in a low amount of cellulose. The hemicelluloses, (secreted in the Golgi apparatus and transported by the Golgi vesicles to the plasma membrane), are deposited at the same time as the cellulose microfibrils in the primary cell wall. The hemicelluloses influence the pattern of the aggregation of the cellulose microfibrils and provide the pattern for the lignin assembly [54]. The lignification, (by condensation of monolignols synthesised in the cytoplasm and transported through the plasma membrane into the cell walls), of cell corners and the middle lamella starts first after accomplished deposition of pectin and started formation of the S_1 cell wall, and is followed by a slow deposition in the P cell wall and the S_1 layer during the S_2 layer formation [55]. It is sometimes difficult to separate the middle lamella from the primary cell wall, which is the reason why the middle lamella and the primary cell wall are often collectively referred to in the literature as the compound middle lamella (CML).

When it comes to the ultrastructure of the primary cell wall, it is suggested that xyloglucan is hydrogen bonded to cellulose (making the basis of a network within the native primary cell wall – *the xyloglucan-cellulose network*) [29]. Xyloglucan molecules are long enough to bind to two neighbouring cellulose molecules and cross-link them. Xyloglucan can also be covalently linked to pectin [21,56]. It is also known that lignin can make covalent cross-links with both protein and pectin [47]. Pectin and protein are linked by ionic bonds and that cellulose and pectin form covalent bonds [31]. Pectin itself can exist as a cross-linked network within the native primary cell wall (by covalent bonding between different pectic polymers, but also through the intermolecular junction zones between HGA and Ca^{2+}, or RG-II and B, the boron di-diesters) – forming *the pectic network*. Protein can also build a cross-linked network through the intermolecular bridges – *the protein network*. To summarize, the primary cell wall is constructed of these three structurally independent but interacting

networks forming the Type I wall [28,29]. It was recently suggested that there are covalent links between lignin and carbohydrates in lignin-carbohydrate complexes (LCCs) in the primary cell wall of softwood [57,58].

3.2 The secondary cell wall

The secondary cell wall is started to develop first after the accomplished growth of the primary cell wall, i.e. its completed radial expansion. At this stage, cells undergo a dramatic shift in production of type of the structural polymers, from polymers supporting the expansion of the protein-rich primary cell wall to polymers supporting the deposition of the cellulose- and hemicellulose-rich secondary cell wall, which will eventually be lignified. The secondary cell wall is deposited inside the primary cell wall, where a gradual formation of the S_1, S_2 and S_3 layers is occurring – *a cell wall thickening* [10]. The gradual formation takes place by the hemicelluloses biosynthesis, secreted in the Golgi apparatus in the cytoplasm and transported by the Golgi vesicles to the plasma membrane. The secreted hemicelluloses absorb water, are cross-linked by Ca^{2+} ions and form a hydrated gel, which covers the innermost surface of a cell wall [55]. The deposition of hemicelluloses occurs at the same tame as the extrusion of the cellulose microfibrils, where the deposited hemicelluloses determine the aggregation pattern of the cellulose microfibrils, and starts before the lignification takes place. The deposited hemicelluloses and cellulose microfibrils determine the pattern of the lignin condensation [55,59]. The deposition of cellulose microfibrils occurs in exposure to the hemicellulose gel increasing the thickness of the cell wall, where the cellulose microfibrils are deposited in a defined direction and will form so-called a honeycomb structure [55]. The cellulose microfibrils are produced by so-called rosette terminal complexes in the plasma membrane; a rosette is composed of sex particles where each of the particle is composed of six sub-units and each of the sub-unit produces one cellulose chain – totally generating 36 cellulose chains, which are assembled into a cellulose microfibril [60]. The deposition of lignin occurs in the presence of the hemicellulose gel; by condensation of monolignols synthesised in the cytoplasm and transported through the plasma membrane into the cell walls – *a lignification*. The monolignols diffuse into the hemicelluloses gel, which fills the space between the cellulose microfibrils, i.e. the honeycomb structure. The monolignols, also with help of ferulic acid, cross-link between each other and with

hemicelluloses and increase the density of the cell wall. Further, water and Ca^{2+} ions are removed toward the inner part of the cell wall via the dehydrogenative polymerisation (DHP), or condensation of lignin, and hydrophobic lignin-carbohydrate complexes are formed. The three-dimensional structure of lignin is formed by no random but structurally ordered condensation process [55,61]. The lignification proceeds in three stages: (a) the cell corners and the middle lamella undergo the lignification, but first after the S_1 layer starts to form, (b) during the S_2 layer formation, the lignification is occurring in the P wall and in the S_1 layer, and (c) after that the S_3 layer has formed, the most active lignification occurs though the secondary walls [55,62]. The last stage in the tracheid development is decomposition and disappearance of cytoplasmic content – *a programmed cell death* [10]. This resulting cell wall is a hard dry tube having ability to resistant various stresses.

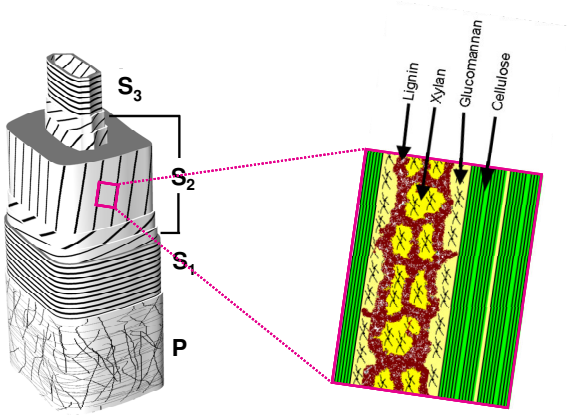

***Figure 14**: Schematic picture of the structure of a softwood tracheid where the ultrastructural organisation of the polymers in the S_2 cell wall is shown, adopted from illustration of the cell wall as illustrated by Brändström [52] and of the S_2 cell wall ultrastructure as illustrated by Salmén and Olsson [11].*

A lot of work has been performed to clarify the interactions between the secondary cell wall constituent polymers. A lamella model of the arrangement of cellulose, hemicelluloses and lignin was proposed, where cellulose microfibrils are primarely interacting with a hemicellulose (i.e. glucomannan) and then these fibrillar formations are embedded in an amorphous matrix of remaining hemicelluloses and lignin [24,63,64]. Cellulose and hemicellulose are non-covalently bonded (i.e. hydrogen bounded) to each other [31,65], while lignin and hemicellulose are covalently bonded [66]. Åkerholm, Salmén and Olsson made a detailed research on the interactions between the polymers in the secondary cell wall of the softwood fibre. The authors suggested a different

organisation of the two hemicelluloses. They found that there was strong interactions between cellulose and glucomannan and that xylan interact with lignin [11,67,68] (Figure 14). The existence of covalent linkages between lignin and carbohydrates in the lignin-carbohydrate complexes (LCCs) in softwood was also reported [57,58,69-71].

Orientation of the polymers in the S_2 layer is of importance for the functional characteristics of the entire cell wall, because the S_2 layer occupies 75% - 85% [26] of the total thickness of the cell wall. It is well known that the cellulose chains are mainly arranged in a more or less parallel direction (0° to 30°) to the fibre axis in the major part of the fibre wall, i.e. the S_2 layer [65,67,72-76]. The orientation of the hemicelluloses and lignin is determined by the orientation of the cellulose microfibrils [65,75,76]. It was reported that many of the hemicellulose molecules are oriented in parallel with cellulose and that they coat the cellulose microfibrils, while other hemicellulose molecules are randomly dispersed in the space between the cellulose microfibrils [77], and/or one molecule of the hemicellulose can be partly attached to cellulose microfibril with the portions that can extend into the matrix and covalently bond to lignin [65]. Some evidence also exists that points to that the glucomannan is oriented along these cellulose microfibrils in softwood [65,67,74]. Less is known about the extent to which the xylan has an orientation. From the newer studies, made in our lab, it was seen that xylan in hardwood is oriented parallel to the cellulose microfibrils [75], and also xylan from branches of softwood and hardwood is oriented parallel to the cellulose microfibrils [74]. With regard to lignin, it has been shown that there is an orientation in the plane of the cell wall surface, i.e. tangential orientation [78], whereas indications for an orientation of the phenyl propane units along fibres in softwood are less clear [79]. The proposed parallel arrangement of hemicelluloses may impose a degree of order of the lignin [77]. Recently, it was shown that the lignin in hardwood is highly oriented, i.e. parallel to the cellulose microfibrils [75], also lignin from branches of softwood and hardwood is oriented parallel to the cellulose microfibrils [74], while the lignin from the middle lamella of softwood shows no orientation, i.e. it is isotropic [76].

4 BIOCOMPOSITES

There is an increasing interest in substituting today's films for many applications, such as food packaging applications, with films based on renewable resources. In general, today's food packaging materials are based on fossil resources, and consequently one of the reasons for the increasing amount of pollution concerning the increasing amount of CO_2 in nature. Hence, an increasing concern for sustainability of resources and preservation of environment are distinguished. On these bases, consumers can have an extremely positive view on biodegradable and sustainable packaging materials. Biocomposites, based on nanocelluloses: bacterial cellulose (BC) and spruce/pine microfibrillated cellulose (MFC), and hemicelluloses: rye arabinoxylan (rAX) and spruce galactoglucomannan (GGM), may thus be potential alternatives for future food packaging materials. These polymers come from renewable resources, are totally biodegradable and recyclable, have potentially low cost, are CO_2 neutral when concerning global warming, have good mechanical performance at minimum weight and so on. Both components, celluloses and hemicelluloses, come from non-food sources which is one additional advantage of their usage for this purpose in comparison for example with starch or proteins. Polar biopolymers, such as xylans, are found to be good barriers against lipids. They have a possibility to form dense networks, and as such show good gas barrier properties. On the other hand, as hydrophilic biopolymers, hemicelluloses are sensitive to moisture and this disadvantage, which leads to poor dimensional stability of their films, has to be improved. In addition, the strength and flexibility of the hemicellulose films has to be improved, a fact addressed by introducing nanocellulose as a reinforcing phase when preparing the biobased nanocomposite films.

4.1 Biomimicking

Nature creates high performance materials where the plant cell wall is one of the most interesting when concerning its ability to resist various internal and external stresses. In the plant cell walls, cellulose is the principal reinforcing component in cross-linked networks of hemicelluloses, lignin and sometimes pectin and protein. Hemicelluloses, through their unsubstituted regions of backbones, interact with cellulose by intermolecular hydrogen bonding in both annual and woody plants [21,28]. This interacting ability of these two components can be mimicked in order to create new

plant inspired materials based on renewable resources. Nature, in general, can serve as an astonishing source, supplying both the raw material and inspiration when designing the future materials for targeted usage. The great advantage in using BC as a model for plant cellulose lies in its high purity and relatively easy synthesis as well as in a fact that its chemical structure is the same as of wood cellulose. The advantage of using rye AX as a matrix model component is that it represents non-food fraction of a cereal cell wall as well as a potential agricultural waste, and also, that it is available on market where no additional isolation procedure is needed. An additional advantage of using rye AX is that its chemical structure is quite similar to the chemical structure of softwood xylan. On the other hand, MFC (i.e. cellulosic nanofibrils disintegrated from the plant cell walls of spruce/pine wood pulp) and GGM (that can be recovered, among others, from process water in TMP production from spruce wood), are biopolymers that originate from wood and therefore are considered as attractive reinforcement and matrix components, respectively. In addition, these raw materials are from renewable resources and are completely biodegradable. The BC and MFC have nanoscale lateral dimensions which enhance mechanical properties of the final materials, and the casting of cellulose/hemicellulose composites can be carried out in water at ambient temperature and pressure. By accomplishment of desired properties of cellulose/hemicellulose films, an increased use of biobased materials in the production of advanced packaging materials can be expected. Further, this can contribute to the global efforts to increase the use of renewable resources instead of oil and petrochemicals, and finally help with regard to the environmental but also the economical issues.

5 EXPERIMENTAL

5.1 Materials

5.1.1 Primary cell wall material

Primary cell wall material was prepared by decrilling and fractionation of a first stage thermomechanical pulp (TMP) of Norway spruce (*Picea abies*) from a Swedish pulp mill. The present ray cells were separated from resulting fines fraction (particle size < 50 µm), which was then highly enriched on primary cell wall, while some ray cells and pit structures were remaining (see Figure 15) (for more details see PAPER I).

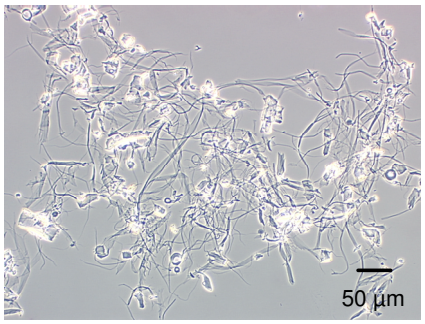

***Figure 15**: Light microscope micrograph, illustrating the primary cell wall material after fractionation and separation from the ray cells. The scale bar is 50 µm.*

5.1.2 Sulphonated primary cell wall material

Sulphonated primary cell wall material was prepared from a first stage low degree sulphonated pulp. Here, sapwood chips of Norway spruce (*Picea abies*), from a saw mill, were first sulphonated by impregnation to a level of 0.11 % (calculated as the weight of Na_2SO_3 on the oven dry weight of the chips).

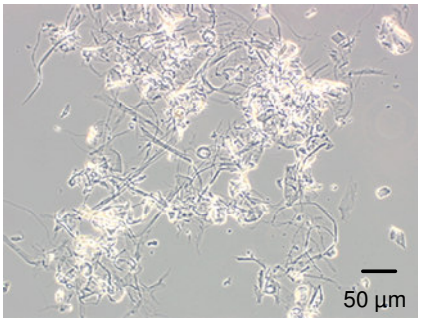

***Figure 16**: Light microscope micrograph, illustrating the sulphonated primary cell wall material after fractionation and separation from the ray cells. The scale bar is 50 µm.*

The low degree sulphonated chips were refined in a pilot refiner. A first stage low degree sulphonated pulp was processed by decrilling and fractionation followed by separation from the ray cells. Resulting sulphonated primary cell wall material was highly enriched on primary cell wall, while some ray cells and pit structures were remaining (see Figure 16) (for more details see PAPER III).

5.1.3 Secondary cell wall material

Wood fibres (W) were prepared as mechanically altered Norway spruce (*Picea abies*) fibres, so that they only had the secondary cell walls of S_2 and S_3 (Figure 17). The thickness of the S_3 layer is 5% of the thickness of the S_2 layer, on average. This is the reason why it is possible to state that these fibres might acceptably represent the properties of the S_2 layer. These fibres were prepared from a first stage TMP, which was treated mechanically in a disintegrator to remove the outer layers of the fibre walls, i.e. ML, P and S_1.

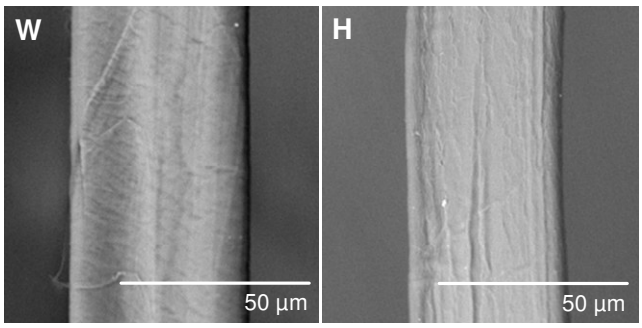

***Figure 17**: ESEM micrographs, illustrating a wood fibre (W) and a holocellulose fibre (H). The scale bar is 50 µm.*

Holocellulose, i.e. delignified fibres, (H), chemically altered fibres, were prepared from Norway spruce (*Picea abies*) chips, using a chemical isolation process, called a maceration process [80]. In this process, in addition to the removal of the lignin, approx. 45% of the content of the hemicelluloses in the wood was removed. In the process the outer layers of the fibre wall, i.e. ML, P and S_1, were removed living the secondary cell wall of S_2 exposed (Figure 17).

5.1.4 Model components

5.1.4.1 Rye arabinoxylan (rAX)

Cereal cell walls, such as from rye (*Secale cereale* L.), are rich in arabinoxylans and therefore an attractive source since they represent non-food fractions and a potential agricultural waste (see section 2.2.3.2). Pure rye arabinoxylan (rAX), which is well characterised, is available on market and no isolation procedure is needed. For these reasons it was chosen as a matrix model compound for this study.

5.1.4.2 Bacterial cellulose (BC)

As already mentioned, cellulose is the most abundant biopolymer on Earth representing the major component of plant biomass, but cellulose can also be synthesised by various bacteria (e.g. *Acetobacter* also named *Gluconacetobacter*, *Aerobacter*, *Azotobacter*, *Rhizobium*, *Agrobacterium* or *Sarcina*) as an extracellular biopolymer, termed as bacterial cellulose (BC). The most efficient bacterium for biosynthesis of BC is *Acetobacter xylinum* (*A. xylinum*), a Gram-negative, rod shaped, aerobic, acetic acid bacterium, naturally occurring on rotten fruits and vegetables. BC is produced by cultivation of *A. xylinum* in an aqueous medium containing sugar source, such as glucose, sucrose, or fructose, as well as various substrates, such as, glycerol, mannitol, or arabitol. *A. xylinum* produces cellulose extracellularly, where 12-16 cellulose chains are extruded from a single bacterial cell into the culture medium as an 1.5 nm thin sub-elementary fibril. Several sub-elementary fibrils aggregate into a microfibril and further a number of microfibrils aggregate into a ribbon-like assembly, 40 nm to 60 nm in a width [81]. Various dimensions for the ribbon assemblies were reported by Brown et al. in 1976 (3.2 nm×133 nm (thickness×width) [82]), and by Zaar in 1977 (3-4 nm×70-80 nm (thickness×width) [83]). The length of the ribbon assemblies was reported to be in a range from 1 µm to 9 µm [84]. The ribbons are then under static conditions formed as a thick, gelatinous pellicle at the air-liquid interface. This pellicle is characterised by the 3D nanofibrillar structure [85] of an ultrafine ribbon network stabilized by extensive hydrogen bonding [84].

BC possesses unique physical, chemical and mechanical properties, such as a high crystallinity (60% to 80%), a high water holding capacity (up to 200 times of its dry

mass), a high mechanical and wet strength, a high DP (2,000-6,000 [83,86]) and great elasticity [87,88] (a Young's modulus of ~30 GPa [89]). BC is similar to native celluloses from higher plants. The chemical composition of the two celluloses is identical, i.e. they are built in form of long linear molecules composed of β-1,4-linked β-D-Glc*p* units in the k_I conformation giving the stable crystalline form, i.e. cellulose I [29], but they differ in the crystalline allomorphs of cellulose I, where the I*α* crystalline form is predominant in BC [90] and the I*β* crystalline form is predominant in native cellulose in higher plants [91]. The dominant crystalline allomorphs of cellulose in the S_2 layer of wood is the I*α* crystalline form (in holocellulose fibres ~60% [92]). BC is extremely pure material that is, unlike plant celluloses, completely free from hemicelluloses and lignin [93]. One particularly interesting difference between the two celluloses is in the size of their microfibrils; the size of the microfibrils in BC is about 100 times smaller than that of plant cellulose. This, in addition to the unique nanofibrillar porous morphology (see Figure 18) and a large surface area of BC, is the main cause for its very high water binding ability [85,87]. These unique properties of the BC were reason for considering the BC as a reinforcement model component in this study.

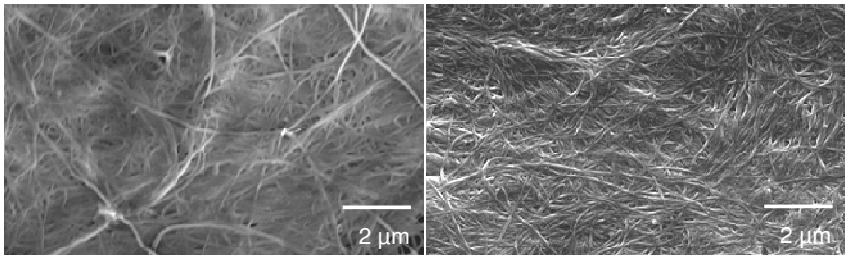

***Figure 18**: SEM micrographs of the microfibrillar network of pure bacterial cellulose, left: freeze dried BC and right: a BC film, representing the nanosized structure of the material. The scale bar is 2 µm.*

5.1.4.3 Spruce galactoglucomannan (GGM)

Galactoglucomannan (GGM) is the most abundant hemicelluloses in the softwood secondary cell wall (see section 2.2.2), but also the main water soluble polysaccharide in process water in the production of TMP from Norway spruce (*Picea abies*). About 5% to 10% of spruce GGM is dissolved during TMP production, hence an increasing interest for the potential recovery of the dissolved GGM. Spruce GGM, used in this study, was obtained, after ethanol precipitation, from process water of a Finnish pulp mill in an isolation trial. Here, GGM was dissolved in water, filtrated, concentrated

and dried [94,95]. The GGM is an interesting and potential raw material for using in biomimicking of plant cell walls.

5.1.4.4 Spruce/pine microfibrillated cellulose (MFC)

Microfibrillated cellulose (MFC) is a specifically prepared cellulosic material composed of liberated semicrystalline *nanosized* cellulose microfibrils (so-called MFC *nanofibrils*, which should not be confused with *microfibrils* formed during cellulose biosynthesis) with a high aspect ratio (i.e. length to with ratio). The lateral dimension of MFC nanofibrils and nanofibril aggregates is in order of 5 nm to 20 nm, respectively [96] and mostly up to 40 nm due to their ability to aggregate [97] (cf. for kraft pulp fibres, the lateral dimension of microfibrils and microfibril aggregates is about 5 nm and 20 nm, respectively [98]), which highly depends upon the preparation technique used. Most frequently, various chemical and/or enzymatic pre-treatments prior an intensive mechanical fibrillation are used for preparation of the MFC. The pre-treatments are introduced to purify the origin material, from various plant sources, from hemicelluloses and lignin, but also to significantly reduce the energy consumption during the microfibril liberation process [99]. The MFC was first introduced by Turbak et al. [100] and Herrick et al. [101], while the first carboxymethylated MFC was manufactured by Wågberg et al. [102]. An improved MFC was prepared by Pääkkö et al. [96] using a combination of mechanical and enzymatic treatments, and introducing high-pressure homogenization technique. An enhanced carboxymethylated MFC was prepared by Wågberg et al. [103] using a high-pressure homogenisation followed by ultrasonication and centrifugation. Here, a commercial sulfite softwood dissolving pulp, from a Swedish pulp mill, was used as a starting material (60% Norwegian spruce (*Picea abies*) and 40% Scottish pine (*Pinus sylvestris*)), containing less than 5% of hemicellulose and less than 1% of lignin. Wågberg et al. reported that in this MFC, nanofibrils and nanofibril bundles were present with a width of 5 nm to 15 nm and length of up to 1 µm, a DP of about 1100 and a charge density of 0.5 meq.g^{-1}, which additionally improved the liberation process of cellulose microfibrils due to the repulsion of the introduced carboxylate ions by carboxymethylation (cf. the charge density of cellulose in native fibres is close to 0). The introducing of this chemical pre-treatment reduced the energy consumption by 98%, hence an increasing interest for commercial production. These MFC nanofibrils were strongly entangled in a disordered network forming a MFC gel,

where also inter-fibrillar hydrogen bonding is present. However, this particular MFC, in a form of a film, was characterised in detail by Plackett et al. (with a Young's modulus of ~5 GPa) [104], and Siró et al. (with a Young's modulus of ~7 GPa) [105] but then the material was additionally treated by multiple homogenisation steps.

The MFC used in this study is similar to the carboxymethylated MFC prepared by high-pressure homogenisation [103], with an exception: the dispersion was made by homogenisation instead of above mentioned ultrasonication and centrifugation. This material was chosen as a reinforcement model component, due to its unique properties: high strength and stiffness, low density, good barrier properties, biodegradability and renewability. The fact that the lateral dimension of the MFC is ranging in nanoscale is of essential importance when preparing the nanocomposites (see Figure 19). Probably, the most interesting property of the MFC is that it comes from a woody source because of a developing interest to prepare new materials based on polysaccharides from wood.

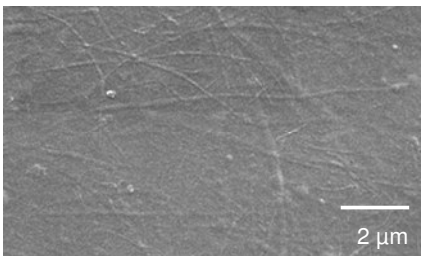

***Figure 19**: SEM micrograph of the microfibrillar network of pure microfibrillated cellulose, a MFC film, representing the nanosized structure of the material. The scale bar is 2 µm.*

5.1.5 Cellulose/Hemicellulose model systems

The interacting ability between cellulose and hemicellulose was mimicked in order to create cellulose/hemicellulose model systems for future packaging materials. In this study, three series of cellulose/hemicellulose model systems were prepared according to Table 1. In series a) rye arabinoxylan (rAX), Ara/Xyl ratio of 0.50, was reinforced with bacterial cellulose (BC) (0%, 5% and 15% w/w), while in series b) debranched rye arabinoxylan (rDAX), Ara/Xyl ratio of 0.16, was reinforced with bacterial cellulose (BC) (0%, 5% and 15% w/w). In series c) spruce galactoglucomannan (GGM) was reinforced with spruce/pine microfibrillated cellulose (MFC) (0% and

15% w/w) and here glycerol was added as plasticiser (10%, 20%, 30% and 40% w/w of GGM).

***Table 1**: Codes and descriptions of: a) rAX, b) rDAX and c) GGM films studied.*

Code	*Description*
a)	
rAX	100% arabinoxylan (Ara/Xyl ratio = 0.50)
rAX:5BC	95% arabinoxylan + 5% fibrillated bacterial cellulose
rAX:15BC	85% arabinoxylan + 15% fibrillated bacterial cellulose
b)	
rDAX	100% debranched arabinoxylan (Ara/Xyl ratio = 0.16)
rDAX:5BC	95% debranched arabinoxylan + 5% fibrillated bacterial cellulose
rDAX:15BC	85% debranched arabinoxylan + 15% fibrillated bacterial cellulose
c)	
GGM/40gly	100% galactoglucomannan + 40% glycerol
GGM/30gly	100% galactoglucomannan + 30% glycerol
GGM/20gly	100% galactoglucomannan + 20% glycerol
GGM:15MFC/40gly	85% galactoglucomannan + 15% microfibrillated cellulose + 40% glycerol
GGM:15MFC/30gly	85% galactoglucomannan + 15% microfibrillated cellulose + 30% glycerol
GGM:15MFC/20gly	85% galactoglucomannan + 15% microfibrillated cellulose + 20% glycerol
GGM:15MFC/10gly	85% galactoglucomannan + 15% microfibrillated cellulose + 10% glycerol

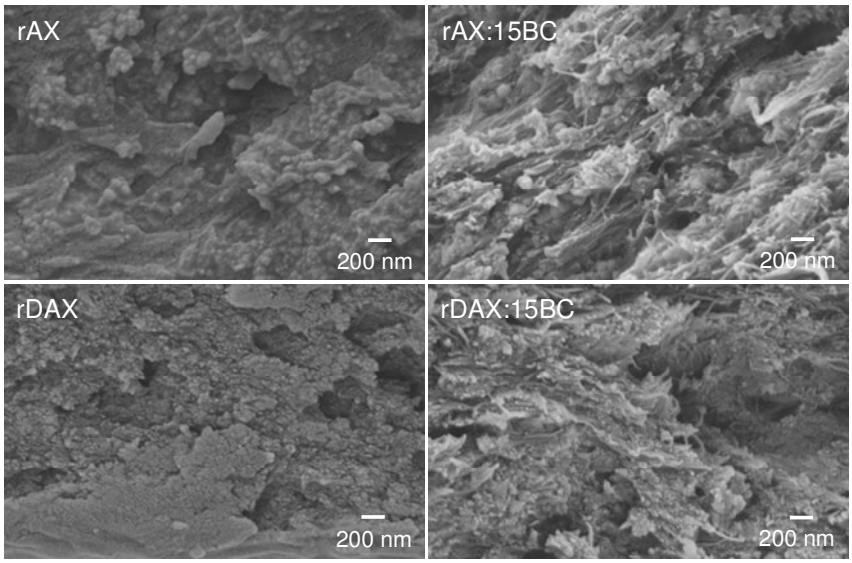

***Figure 20**: SEM micrographs of fracture surfaces of rye arabinoxylan films, unmodified rAX and enzymatically modified rDAX, and corresponding composite films with 15% (w/w) bacterial cellulose. The scale bar is 200 nm.*

Figure 20 shows SEM micrographs of the fracture surfaces of representative films. The micrographs of the pure rAX and rDAX films show quite homogenous structures, where the debranched arabinoxylan formed smaller aggregated particles than the unmodified arabinoxylan. In the composite films the fibrous phase of reinforcing bacterial cellulose was more aggregated in the rAX:15BC film than in the rDAX:15BC. This could be explained by an improved interaction between the arabinoxylan and BC occurring when the arabinose units were removed.

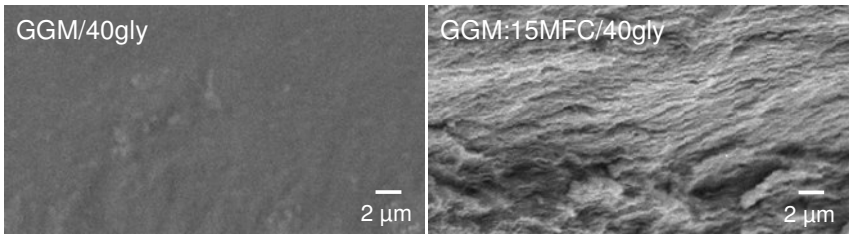

***Figure 21**: SEM micrographs of cross-sections of films from GGM/40gly and GGM:15MFC/40gly. The scale bar is 2 µm.*

Figure 21 shows SEM images of the cross-section of the pure GGM film and the composite film with 15% of MFC, both plasticised with glycerol (40 wt% of the weight of GGM). The GGM film had a relatively smooth cross section. In contrast, the cross section of composite film with 15% MFC was rougher and layered. Both films showed quite homogenous structures.

5.2 Methods

5.2.1 Dynamic FTIR spectroscopy

Infrared (IR) spectroscopy is an important tool for the characterisation of the chemical and physical nature of polymeric materials. It is based on the principal that a molecule absorbs IR radiation at a specific frequency, exciting it into a higher energy stage. The IR radiation beam covers a broad frequency range. When this radiation goes through a sample, the energy, at certain frequencies, is absorbed by the sample. As a result of this absorption, a graph of the energy absorbed plotted against the frequency is obtained. This graph is termed a spectrum, where the characteristics of different molecular motions are specified. Fourier transform (FT) infrared spectroscopy is based on measuring the absorbance as a function of time, i.e. the time-domain spectroscopy, while conventional spectroscopy is based on measuring the absorbance as a function of the frequency or wavelength, i.e. the frequency-domain spectroscopy. One time-domain spectrum contains the same information as one frequency-domain spectrum and these spectra can be converted (or *modulated*) to each other using mathematical manipulations.

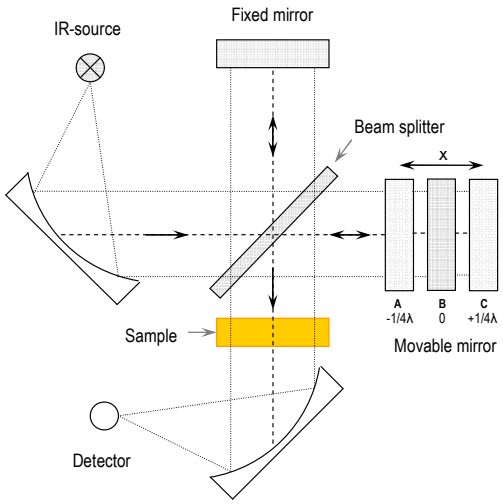

***Figure 22**: Schematic chard of the Michelson Interferometer.*

The Michelson interferometer is a device for modulating of the optical radiation. By a beamsplitter, a beam of the incident radiation containing all wavelengths splits into two equal beams. One beam is partially reflected to the fixed mirror and partially transmitted to the movable mirror. The beams are then reflected from mirrors and they

again meet the beamsplitter, where they recombine. Here, two halves of these beams are directed toward the sample and afterwards toward the detector, while the other halves of beams are reflected back toward the source. The two halves passing the detector through the sample contain the analytical information about the sample, whereas the other two halves contain information about the source. The two beams are recombined in such a way that the intensity variation of the combined beam can be measured as a function of difference in the length of the parts of the two halves. When the mirrors are equidistant from the beamsplitter (position B in Figure 22) the two halves of the recombined beam will be totally in-phase, the power will be a maximum and a constructive interference occurs. But, the motion of the movable mirror (by a distance equal to exactly one-quarter wavelength, -¼λ at position A or +¼λ at position C in Figure 22) will change the path length of the corresponding reflected beam by one-half wavelength (one-quarter wavelength for each direction) and a destructive interference occurs. The destructive interference will then reduce the power of the recombined beam to zero and the two halves of the recombined beam will be totally out-of-phase. Further motion will bring the two halves back in-phase so that the constructive interference can again occur. This difference is termed as the displacement of the movable mirror or the *retardation*, *x*. This means that the signal is recorded in the time-domain spectra. The plot of the output power from the detector versus x is called an *interferogram.* The interferogram is then converted into the frequency-domain spectra – the FTIR spectra – by applying the *Fourier transformation*:

$$S(\nu) = 2\int_{-\infty}^{\infty} I(x)\cos(2\pi\nu x)dx, \qquad (1)$$

where $S(\nu)$ is the intensity at wavenumber, ν, $I(x)$ is the radiation intensity dependent on the retardation, *x*. Wavenumber can be converted into wavelength and frequency:

$$\nu[1/cm] = \frac{1}{\lambda[cm]} = \frac{\omega[1/s]}{c[cm/s]}, \qquad (2)$$

where ν is the wavenumber, λ is the wavelength, ω is the frequency if the radiation and c is the velocity of light ($3\times10^{10}\ cm/s$).

The FT instrument based on the Michelson interferometer must include a *laser* (HeNe laser) to establish the zero retardation. One precisely *drive mechanism* is needed, because the velocity of the moving mirror must be constant and its position must be exactly defined. Most common resolutions (equally spaced frequency or wavelength intervals) of the FT instruments are from 8 cm^{-1} to 0.01 cm^{-1}. The *beamsplitter* used for work in the mid-IR region is made of thin film of germanium (Ge) deposed on potassium bromide (KBr). The *detectors* used for the mid-IR region are the deuterated triglycine sulphate, $(NH_2CH_2COOH)_3{\cdot}H_2SO_4$, (DTGS) – a thin pyroelectric crystal operating at room temperature, and the liquid-nitrogen-cooled mercury cadmium telluride, HgCdTe, (MCT) detector, which has a very rapid response and a high sensitivity. And finally, the *IR-source* used for mid-IR region is the standard ceramic located in the water-cooled tower. It consists of an inert solid that is electrically heated to a temperature between 1500 K and 2200 K approaching the energy of a blackbody [106].

There are three major advantages, which made the FT instruments very useful, (1) the first is the *optical throughput* or *Jaquinot advantage*, a construction with no slits in the FT instruments making the greater power and sensitivity of the IR radiation, (2) the second advantage (*Connes advantage*) of the FT instruments is an extremely high wavelength precision and (3) the third advantage of the FT instruments is that all elements of the signal, emitted by the polychromatic IR-source, reach the detector simultaneously. This decreases the observation time in FTS measurements (1s or less). This advantage is often called the *multiplex* or *Fellgett advantage*[106].

5.2.1.1 Theory of dynamic FTIR spectroscopy

The dynamic FTIR spectroscopy technique is based on a combination of the FTIR spectroscopy with the dynamic mechanical analysis (DMA). This measuring technique is useful for studying molecular interactions in complex polymeric systems, where the macroscopic properties, i.e. viscoelasticity, of the polymeric material are closely coupled to submolecular cooperation, i.e. ultrastructure, depending on the local environment in this polymeric material. An external perturbation, i.e. a non-

destructive sinusoidal strain with very low amplitude (~55 μm), less than 0.3% of the sample length, is applied to the polymeric material and causes reversible stress-induced reorientational changes on the molecular level. Changes in submolecular reorientation are closely influenced by molecular interactions occurring in the material and can be related to the viscoelastic behaviour of the material [9]. Firstly, the absorption of the incident IR radiation occurs if the frequency of the electric field vector of this incident radiation is in resonance with the vibrational frequency of the electric dipole-transition moment of the particular molecular vibration. Secondly, the absorption of the incident IR light takes place if the electric field vector of the incident radiation and the electric dipole-transition moment of the particular molecular vibration are oriented parallel, with respect to each other [107]. That is an important aspect since a polariser is used in this technique (see Figure 23).

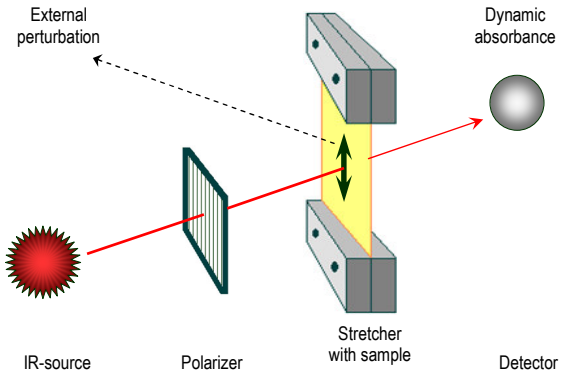

***Figure 23**: Schematic diagram of the dynamic FTIR spectroscopy experiment.*

The polariser is used in either a 0° or a 90° polarisation mode. This means that the IR radiation is absorbed either in a parallel or a perpendicular direction to the stretching direction [108-110]. The molecules that interact are thought to move in-phase with each other and, with the applied strain, to show an elastic response of the material, while molecules that do not interact are likely to move independently or 90° out-of-phase with the applied strain, showing a viscous response of the material. For a given dynamic strain, $\tilde{\varepsilon}(t)$ with small amplitude, $\hat{\varepsilon}$ and frequency, ω:

$$\tilde{\varepsilon}(t) = \hat{\varepsilon} \sin \omega t, \qquad (3)$$

the time-resolved spectral response of the material, $\tilde{A}(\nu, t)$ is represented as a function of wavenumber, ν:

$$\tilde{A}(\nu,t) = A'(\nu)\sin\omega t + A''(\nu)\cos\omega t, \tag{4}$$

where $A'(\nu)$ characterises the in-phase spectrum, i.e. the absorbance variations that are in-phase with the applied dynamic strain and $A''(\nu)$ signifies the out-of-phase spectrum that represents the absorbance variations which are 90° out-of-phase with the applied external perturbation [111,112]. These two components can be further coupled to a magnitude spectrum, $\hat{A}(\nu)$ and a phase spectrum, i.e. a phase loss angle for each wavenumber, $\delta(\nu)$ and expressed as the following (cf. Figure 24):

$$A'(\nu) = \hat{A}(\nu)\cos\delta(\nu), \tag{5}$$

$$A''(\nu) = \hat{A}(\nu)\sin\delta(\nu), \tag{6}$$

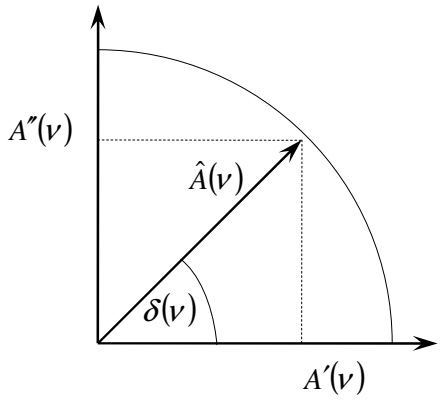

***Figure 24**: Vector presentation of the in-phase, out-of-phase, magnitude and phase spectra.*

$$\hat{A}(\nu) = \sqrt{A'(\nu)^2 + A''(\nu)^2}\ , \tag{7}$$

$$\delta(\nu) = \arctan\left(\frac{A''(\nu)}{A'(\nu)}\right). \tag{8}$$

The magnitude spectrum, $\hat{A}(\nu)$, represents the amount of induced absorption change for each wavenumber, while the phase spectrum, $\delta(\nu)$, represents the phase delay for each wavenumber [113,114].

5.2.1.2 Theory of dynamic 2D FTIR spectroscopy

The dynamic 2D FTIR spectrum provides useful information about various intermolecular and intramolecular interactions, which influence the reorientability of functional groups in a polymer material. The advantage of this technique is the possibility of resolving the overlapping peaks in a spectrum, by spreading peaks over the third dimension. The 2D spectra are obtained as a function of two independent wavenumbers (on the *x* and *y* axes), allowing a selective cross-correlation analysis of 2D signals (the correlation intensities on the *z* axis), by applying the following equations:

$$X(\tau) = \Phi(\nu_1, \nu_2)\cos \omega t + \Psi(\nu_1, \nu_2)\sin \omega t, \quad (9)$$

$$\Phi(\nu_1, \nu_2) = \frac{1}{2}[A'(\nu_1)A'(\nu_2) + A''(\nu_1)A''(\nu_2)], \quad (10)$$

$$\Psi(\nu_1, \nu_2) = \frac{1}{2}[A''(\nu_1)A'(\nu_2) - A'(\nu_1)A''(\nu_2)], \quad (11)$$

where $X(\tau)$ is the dynamic IR cross-correlation function, τ is the correlation time, ω is the frequency of the external sinusoidal perturbation, $\Phi(\nu_1, \nu_2)$ and $\Psi(\nu_1, \nu_2)$ are the synchronous and asynchronous correlation intensities of the dynamic spectrum, respectively, $A'(\nu)$ and $A''(\nu)$ are the orthogonal components, in-phase and out-of-phase of the dynamic spectra, respectively, and ν_1 and ν_2 are two different wavenumbers [9,111,112,115].

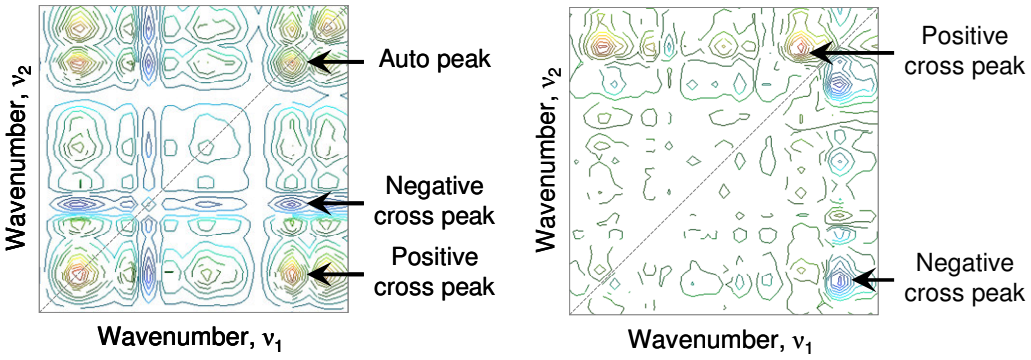

***Figure 25**: (a) Synchronous spectrum and (b) asynchronous spectrum of primary cell wall material, illustrating strong peaks.*

The synchronous correlation spectrum shows the correspondence for the changes in vibration with the same phase (in-phase) and is symmetrical with respect to the diagonal line. The peaks appearing on the diagonal line in a synchronous spectrum are called *auto-peaks*. They are always positive. These auto-peaks indicate the transition dipoles, i.e. functional groups, which have an orientational response to the perturbation. Off-diagonal peaks, called *cross-peaks*, can be either positive or negative. Positive cross-peaks indicate that the changes in the two wavenumbers are in-phase and that the two corresponding dipole moments are reoriented parallel to each other. The negative cross-peaks indicate that the changes in the two wavenumbers are 180° out-of-phase with each other and that the two corresponding dipole moments reorient perpendicularly to each other. The cross-peaks in a synchronous spectrum generally specify that interactions among different polymers occur in the composite material (see Figure 25a above). The asynchronous correlation spectrum shows the correlation for changes with a 90° phase difference (out-of-phase) and is asymmetric in respect to the diagonal line. There are no auto-peaks and no cross-peaks that identify any elastic response of the material. The cross-peaks in an asynchronous spectrum usually signify an absence of strong chemical interactions (see Figure 25b above) [112].

5.2.2 *Imaging FTIR microscopy*

Imaging FTIR microscopy is based on a combination of the static FTIR spectroscopy with the light microscopy, where a sample stage is integrated to the microscopy devise. In the case of the equipment used in this study (a PerkinElmer Spotlight 400), the sample stage is moving in small steps of 6.25 µm under a continuous scanning with mid-IR radiation. This, together with specially designed optics in the microscope and a specially designed detector, i.e. a linear array 6.25 µm MCT detector, (Figure 26a), allows that a sample is scanned over a desired area (Figure 27), which as a result gives an IR full-spectral image including the spectral information (Figure 26c). This means that a sample is analysed locally, down to micrometer scale with a pixel resolution of 6.25 µm, where one pixel has a size of 6.25 µm×6.25 µm (Figure 26a) from which one spectrum is collected. A visible CCD (charge-coupled device) camera is also integrated here, which gives the possibility to generate a visible image of the scanned sample (Figure 26b), where the IR image correspondents to the visible image completely.

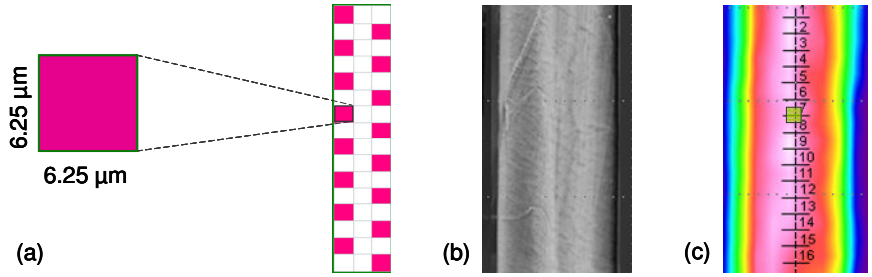

***Figure 26**: (a) schematic image of the linear array detector containing 16 MCT detectors, also showing one magnified pixel of a 6.25 µm×6.25 µm, (b) visible image of a part of a fibre and (c) IR full-spectral image of the same part of a fibre, also showing 16 pixels selected from which 16 spectra can be analysed. A pixel number 7 that correspondents to the pixel magnified in (a) is highlighted here.*

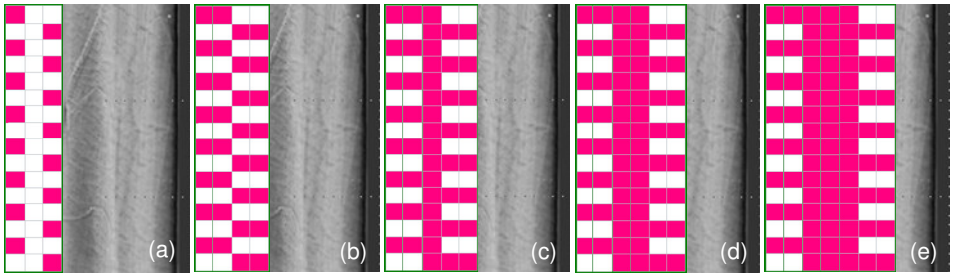

***Figure 27**: Schematic image illustrating the continuous scanning of a part of a fibre, step by step: (a) the first step, (b) the second step, (c) the third step, etc.*

There is also a possibility of performing IR scanning with a polarisation, where the incident IR radiation is polarised by a gold wire grid polariser, in our case, from 0° to 90° polarisation and in relation to the fibre orientation with intervals of 5°. In this way, it is possible to investigate, for example, orientations of different polymers in a wood fibre. If the FTIR spectra were recorded in two polarisation directions, i.e. 0° and 90°, then an orientation spectrum can be calculated using a ratio function (Equation (12)). This determines if vibration of one functional group, and further a polymer possessing this functional group, is oriented more or less parallel or perpendicular to a reference orientation, which is often parallel to 0° polarisation direction:

$$R = \log \frac{T_{90°}}{T_{0°}} \tag{12}$$

where R is the ratio spectra, i.e. the orientation spectra, $T_{0°}$ is the transmission spectra recorded at 0° and $T_{90°}$ is the transmission spectra recorded at 90°. For more precise determination of the orientation of different polymers, Equation (13) can be used:

$$RA = \left(\frac{I_P - I_{\min}}{I_{\max} - I_{\min}} \right) \tag{13}$$

where RA is the relative absorbance, I_P is the intensity of the absorbed IR radiation at a given angle of the polarisation, P, $I_{\max}$ is the maximal intensity observed for a given vibration and $I_{\min}$ is the minimal intensity observed for a given vibration. Here, the relative absorbance values are presented in relation to the angle of the incident IR polarisation (from 0° to 90°).

5.2.3 Dynamic mechanical analysis

The dynamic mechanical analysis (DMA), also called mechanical spectroscopy, is a technique useful for studying the viscoelastic properties in polymeric systems. Basically, a small deformation, i.e. sinusoidal force, is applied to a sample of known geometry under controlled temperature, time, stress, frequency or, in our case, relative humidity (RH) (due to the significant effects of humidity on the mechanical properties of wood polymers). The experiment, i.e. *humidity scan*, is performed in tension mode at a humidity range of 1% to 90% of RH with rate of 1 RH/5 min or 1RH/3 min, a strain amplitude of 8 µm or 5 µm, a frequency of 1 Hz, a temperature of 30 °C and an adjusted static force of 120% to dynamic force. Here, a humidity generator is integrated to the DMA equipment (see Figure 28). The sample is responding to the dynamic force, which is further related to the stiffness (storage modulus, E') and damping (loss tangent, $\tan\delta$) of the material studied.

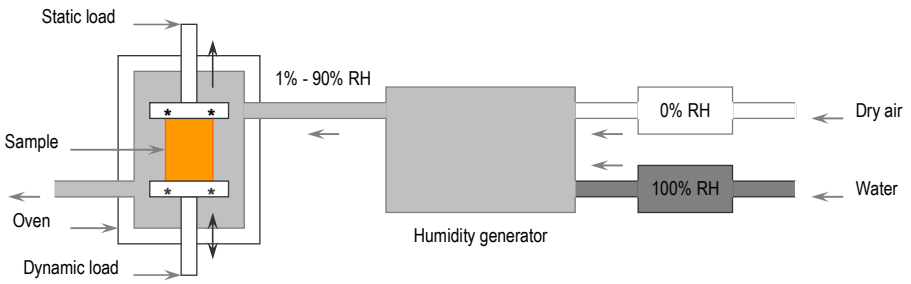

***Figure 28**: Schematic diagram of the dynamic mechanical analysis experiment in tension mode, suitable for studying of polymer films or composite films.*

This measuring equipment can be used for a static mechanical analysis in tension mode, i.e. tensile testing or *stress-strain scan*, at a humidity of 50% RH, a temperature of 30 °C and a static force with a rate of 500 mN/1 min. The sample is responding to this static force, which is further related to the stiffness (Young's modulus, E), strength or tensile strength (stress, σ) and elongation, (strain, ε) of the material studied. Here, the elasticity, E, is determined from slope of the linear part (up to $\varepsilon = 1$) of a stress-strain curve.

5.2.3.1 Theory of dynamic mechanical analysis

Different materials, when exposed to an external deformation, show various responding behaviour, which is also highly dependent on the environmental

conditions, time scale of the deformation and loading pattern. A purely *elastic* material will store the applied force in a form of a potential energy during the loading and once when the load is removed this energy will be completely recovered. This is described by Hooke's law, where the stress and strain are in-phase, i.e. $\delta = 0°$, and the ratio of stress to strain is a modulus, E. In contrary, a purely *viscous* material will not return any of the energy stored during the loading. This energy, which is in a form of thermal energy, is lost as a damping once the load is removed. This is described by Newton's law, where the strain is 90° out-of-phase with the stress, i.e. $\delta = 90°$, and the ratio of stress to strain rate is a viscosity, μ. All polymeric materials as well as all the wood polymers show a *viscoelastic* behaviour, showing both the viscous and elastic behaviour. Here, some of the energy stored will be recovered upon the removal of the load, and the rest of the stored energy will disappear in the form of heat by molecular motions.

The viscoelastic response of the material to the dynamic force applied includes a linear component due to only a very small strains included in the experiment. Then, the applied periodic stress, $\sigma(t)$, as a function of time, t, is a force function:

$$\sigma(t) = \sigma_0 \sin \omega t, \tag{14}$$

where σ_0 is maximum stress and ω is angular frequency, the responding strain, $\varepsilon(t)$, can be represented as:

$$\varepsilon(t) = \varepsilon_0 \sin(\omega t - \delta), \tag{15}$$

where ε_0 is maximum strain and δ is phase loss angle between the stress and strain, representing the angle between the in-phase and out-of-phase components in the sinusoidal motion. The quantities that can be further determined are the modulus representing the stiffness of the material and $\tan\delta$ representing the damping of the material. The modulus can be expressed as storage modulus, E', which is the in-phase component or the real part of the complex modulus (see bellow), representing the elastic behaviour of the material or its ability to store energy:

$$E' = \frac{\sigma_0}{\varepsilon_0}\cos\delta, \tag{16}$$

The modulus can further be expressed as and loss modulus, E'', the 90° out-of-phase component or the imaginary part of the complex modulus, representing the viscous behaviour of the material or its ability to dissipate energy converting it to heat by molecular motions:

$$E'' = \frac{\sigma_0}{\varepsilon_0}\sin\delta. \tag{17}$$

These two components can be related to the complex modulus, E^*:

$$E^* = E' + iE'', \tag{18}$$

where $i = \sqrt{-1}$. The vectorial resolution of these components can be represented by a vector diagram, bellow:

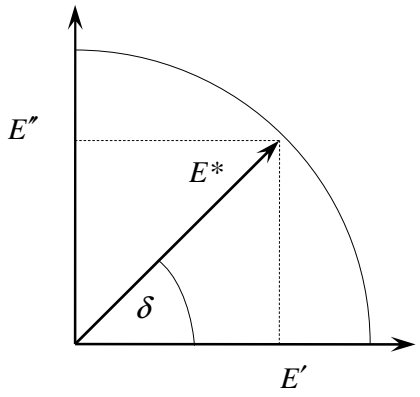

***Figure 29**: Vector presentation of the in-phase, out-of-phase and complex components, and phase angle.*

Note the similarity with the dynamic FTIR spectroscopy (see Section 5.2.1.1). The ratio of the loss modulus to the storage modulus is the loss tangent, $\tan\delta$, also called mechanical loss factor, which is a measure of the damping or the energy dissipation of the material:

$$\tan\delta = \frac{E''}{E'}, \tag{19}$$

which also is independent of the dimensions of a sample measured [116].

5.2.3.2 Viscoelastic behaviour of polymers

Traditionally, the viscoelastic properties of polymeric materials are measured with regard to temperature where they undergo, so called, thermal transitions. There are several thermal transitions present, the *primary transition*, - melting, T_m, the *secondary transition* - glass transition, α, and the *sub-secondary transitions* in glassy state, β and γ, which occur bellow the glass transition temperature, T_g. The glass transition, also termed as softening temperature, where a polymeric material undergoes a transition from its glassy to its rubbery state, occurs only in the amorphous part of the polymer. The T_g can be seen as either a large drop in the storage modulus curve or a peak in the $\tan\delta$ curve with temperature. However, when it comes to wood polymers, it is of highest interest to study the influence of water on the viscoelastic properties. Water is the most common plasticiser in nature. It is well known that water and other plasticisers affect the glass transition temperature of many natural and synthetic amorphous polymers, particularly at low moisture content. A plasticiser is a low molecular component, which, incorporated in a polymer, increases the flexibility of this polymer, and lowers its T_g, melt viscosity, or elastic modulus. A plasticiser causes an increase of the free volume of a polymer by weakening or breaking the intermolecular bonds between polymer chains, which further increases the segmental mobility of polymer chains in the amorphous regions. This is assigned as the main structural relaxation transition, glass transition, α transition, or T_g [117]. In celluloses and hemicelluloses, this transition happens by weakening or breaking the hydrogen bonding between the molecules [118]. Water plasticisation, which influences (i.e. decreases) the α transition, influences also the sub-T_g secondary relaxations, or the β and γ viscoelastic transitions. These transitions happen in the amorphous regions of polymers where only local rotations or vibrations can occur. This means that the β transition involves relaxation of polar, mobile side groups and chains, and the γ transition involves relaxation of short main chain segments [117]. In celluloses and hemicelluloses, the γ transition is attributed to the rotation of the methylol ($-CH_2-OH$) groups of glucose units in cellulose, and the methylol ($-CH_2-OH$) groups

of arabinose, galactose, glucose or mannose units in hemicelluloses. Here, the β transition is associated with the rotation of the methylol-water complexes [119].

6 RESULTS AND DISCUSSION

6.1 Ultrastructural aspects and interactions of the primary cell wall – PAPERS I and II

The primary cell wall of the wood fibre plays an important role for the fibre separation mechanism in the TMP and chemithermomechanical (CTMP) pulping processes. The primary cell wall is the outermost layer of a fibre and has a complex polymeric structure. Its constitutive components are: cellulose, xyloglucan, pectin, protein and lignin. In order to examine the possibilities of affecting this layer for improvement of energy efficiency in mechanical pulping, the viscoelastic behaviour and interactions among its polymers were investigated using dynamic FTIR spectroscopy in combination with dynamic 2D FTIR spectroscopy.

6.1.1 Load-bearing polymers in the primary cell wall

When exposing a polymeric material to an external sinusoidal strain and mid-IR radiation at the same time, a dynamic spectral IR absorbance is achieved. The dynamic spectral response comes from those components in the material that have been actively deformed as result of the applied load. After studying this spectral absorbance, conclusions about the molecular interactions can be made.

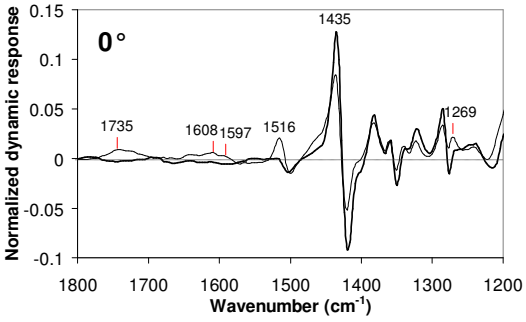

***Figure 30**: Dynamic FTIR in-phase spectra of primary cell wall material (thin line) and TMP (thick line) between 1800 cm^{-1} and 1200 cm^{-1}. The in-phase spectra (elastic response) were recorded at 0% RH, 30 °C and at a 0° polarisation.*

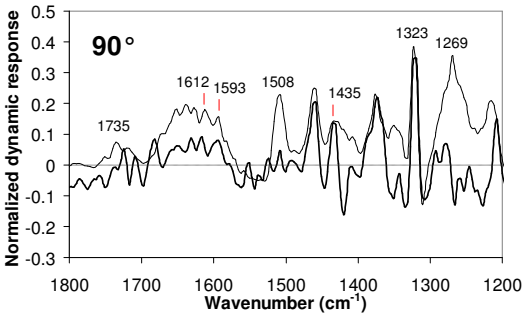

***Figure 31**: Dynamic FTIR in-phase spectra of primary cell wall material (thin line) and CTMP (thick line) between 1800 cm^{-1} and 1200 cm^{-1}. The in-phase spectra (elastic response) were recorded at 90% RH, 30 °C (thin line), 40 °C (thick line) and at a 90° polarisation.*

The elastic responses of the primary cell wall material were compared to elastic response of a spruce TMP (Figure 30) and of a CTMP (Figure 31), respectively, in the interval of 1800 cm^{-1} to 1200 cm^{-1} as examples from two different testing conditions. The primary cell wall material represents the primary cell wall, while both the TMP and the CTMP represent the secondary cell wall material, which means that the elastic response of the primary cell wall is compared with the elastic response of that of the secondary cell wall. The most intense signals at a 0° polarisation were the cellulose C-O-H bending signals at 1435 cm^{-1}, whereas, at a 90° polarisation, the cellulose CH_2 wagging at 1323 cm^{-1} was most dominant [72,92,120]. Thus, as expected, the cellulose was determined as the strongest load-bearing polymer in both the primary and secondary cell walls. Lignin vibrations (the C_{aryl}-O stretching vibrations of methoxyl on phenyl propane units at 1269 cm^{-1} and the lignin C=C aromatic ring vibrations at 1516 cm^{-1}) [79,121-126] occurred as significantly more intense in the primary cell wall than in the secondary cell wall. This illustrates that the lignin from the primary cell wall takes a more active role in load-bearing than the lignin in the secondary cell wall. Hemicellulose signals at 1735 cm^{-1} and 1597/1593 cm^{-1} (C=O stretching vibrations of the carboxylic acid) [127] also seemed to be more intense for the primary cell wall than for the secondary cell wall. Some contribution to the more intense signals, occurring in the wavenumber region of 1665 cm^{-1} to 1550 cm^{-1} for the primary cell wall material, comes from protein vibrations (asymmetric stretching vibrations of the COO^- groups or asymmetric wagging of the NH_3^+ groups) [128] and pectin vibrations (asymmetric stretching vibrations of the COO^- groups from the D-galacturonic acid units, (GalA)) [128]. Peaks seen at 1608/1612 cm^{-1} may correspond to the vibrations of primary amines (the N-H stretching vibrations) [129]. In the wavenumber range between 1650 cm^{-1} and 1590 cm^{-1} the deformation vibrations (scissoring) also occur of the NH_2 groups [129]. Figures 30 and 31 illustrate that the primary cell wall material showed a greater elastic response than the secondary cell wall did, which indicates that there are more interactions among the polymers in the primary cell wall than among those in the secondary cell wall. This can be due to the more organized structure in the secondary cell wall, where cellulose dominates the load-bearing. The measurements suggest that there is an intimately linked network structure among the polymers in the primary cell wall.

6.1.2 *Relative content of cellulose allomorphs in the primary cell wall*

The crystalline cellulose Iα vibration signals usually occur at 3240 cm^{-1} and 750 cm^{-1}, while the crystalline cellulose Iβ signals occur at 3270 cm^{-1} and 710 cm^{-1}. It is obvious, from Figures 32 and 33, that there were no strong signals coming from a cellulose Iα allomorph in the primary cell wall material, whereas Iβ vibration signals were clearly seen. Indeed, clear vibration signal of the cellulose Iβ allomorph was found at 3275 cm^{-1} and also an indication of a vibration signal of the cellulose Iβ allomorph was found at 709 cm^{-1} in the primary cell wall material [127].

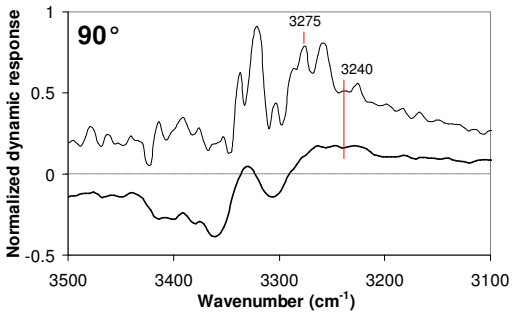

***Figure 32**: Dynamic FTIR in-phase spectra of primary cell wall material (thin line) and TMP (thick line) between 3500 cm^{-1} and 3100 cm^{-1}. The in-phase spectra (elastic response) were recorded at 0% RH, 30 °C and at a 90° polarisation.*

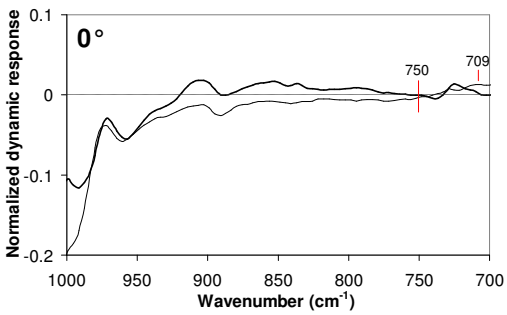

***Figure 33**: Dynamic FTIR in-phase spectra of primary cell wall material (thin line) and TMP (thick line) between 1000 cm^{-1} and 700 cm^{-1}. The in-phase spectra (elastic response) were recorded at 0% RH and 30 °C at a 0° polarisation.*

Further calculations, using the height of the cellulose Iβ peak, H_{710} [92] (cf. Figure 34), indicated that the relative content of cellulose Iβ was around 80% in the primary cell wall. The relative content of the cellulose Iβ in the secondary cell wall was estimated to be approximately 40% [92]. An NMR examination of the cellulose structure of the primary cell wall also showed cellulose Iβ at 88 ppm, in the C4 region, as well as signals at 104 ppm and 106 ppm, while no signals from the cellulose Iα, that usually occur at 89.5 ppm, could be found (see Figure 35). From the spectral fitting of the NMR spectra, the content of the crystalline cellulose in the primary cell wall was determined to be 14%. By taking the sensitivity of the NMR technique into consideration, the relative content of the cellulose Iα, was estimated to be less than 20%. Both the NMR and the dynamic FTIR spectroscopy showed a very good correlation, suggesting a relative high occurrence of cellulose Iβ in the primary cell

wall, when compared to what is observed in the secondary cell wall. This indicated that these cellulose microfibrils were formed in a more stress-free environment than those in the S_2 cell wall.

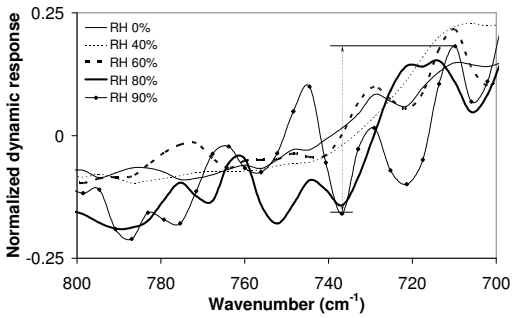

***Figure 34**: Dynamic FTIR in-phase spectra of primary cell wall material, normalised to 1.0 at 1435 cm^{-1}, in the region from 800 cm^{-1} to 700 cm^{-1}, at a 0° polarisation. Measurements were recorded at 0% RH (thin solid line), 40% RH (thin dotted line), 60% RH (thick dotted line), 80% RH (thick solid line) and 90% RH (thin solid line with black squares).*

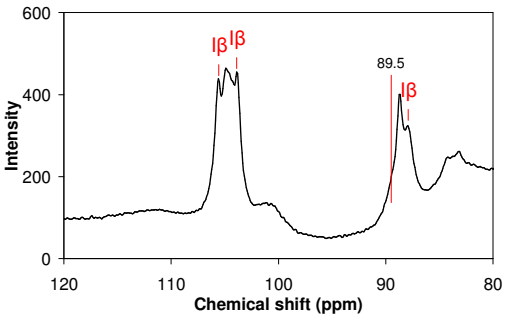

***Figure 35**: Solid state CP/MAS ^{13}C-NMR spectrum of primary cell wall material, illustrating the region of 120 ppm to 80 ppm.*

6.1.3 Interactions among polymers in the primary cell wall

Dynamic 2D FTIR spectroscopy is a technique for making evaluations, especially applicable to the study of molecular interactions. It is based on cross-correlating analysis, which helps to resolve the overlapping vibration bands and, therefore, providing a better understanding of the molecular interactions between a pair of polymers. The 2D spectra for the primary cell wall material, recorded at a 0° polarisation, showed a presence of the cellulose;lignin cross-correlation signals (1435;1269 cm^{-1} and 1435;1516 cm^{-1}) in the synchronous spectrum (Figure 36) and in the asynchronous spectrum (Figure 37). This suggests that cellulose and lignin do not interact when the mechanical load transfer takes place in the primary cell wall.

On the other hand, in the cross-correlating spectra collected at 90° polarisation, an appearance of the cellulose;xyloglucan cross-peaks at 1323;1597 cm^{-1} and 1323;1735 cm^{-1} were observed in the synchronous spectrum (Figure 38), while corresponding signals were absent in the asynchronous spectrum (Figure 39). The cellulose;pectin

signals at 1323;1650-1550 cm^{-1} displayed an analogous pattern. These cross-correlation signals suggest that there are strong interactions between cellulose and xyloglucan, as well as between cellulose and pectin.

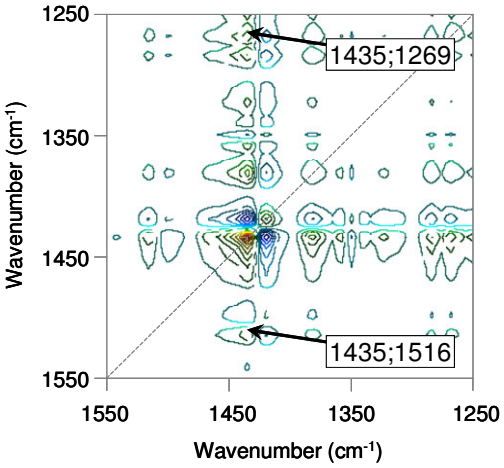

***Figure 36**: Synchronous 2D FTIR spectrum of primary cell wall material recorded at a 0° polarisation, 60% RH and 30 °C, indicating strong cross-peaks at 1435;1269 cm^{-1} and at 1435;1516 cm^{-1} (cellulose;lignin).*

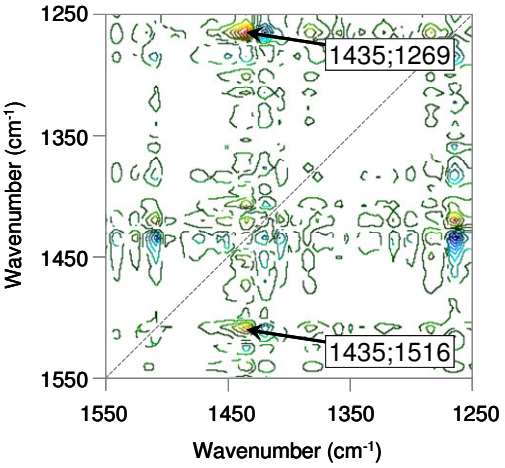

***Figure 37**: Asynchronous 2D FTIR spectrum of primary cell wall material recorded at a 0° polarisation, 60% RH and 30 °C, indicating strong non-correlating cross-peaks at 1435;1269 cm^{-1} and at 1435;1516 cm^{-1} (cellulose;lignin).*

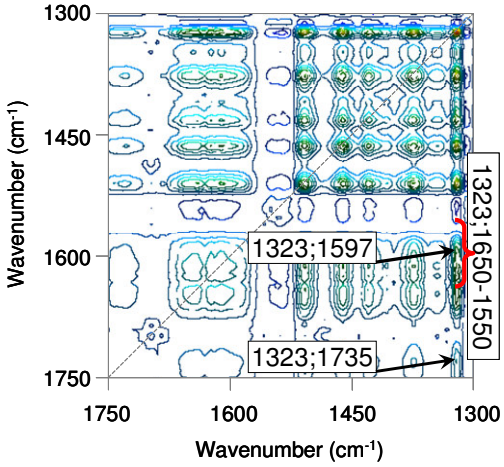

***Figure 38**: Synchronous 2D FTIR spectrum of primary cell wall material recorded at a 90° polarisation, 60% RH and 30 °C, indicating strong cross-peaks at 1323;1597 cm^{-1} and at 1323;1735 cm^{-1} (cellulose; xyloglucan) and cross-peak at 1323;1650-1550 cm^{-1} (cellulose;pectin).*

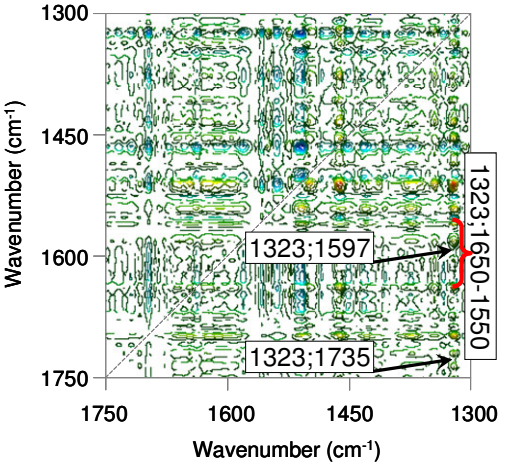

***Figure 39**: Asynchronous 2D FTIR spectrum of primary cell wall material recorded at a 90° polarisation, 60% RH and 30 °C, indicating an absence of cross-peaks at 1323;1597 cm^{-1} and at 1323;1735 cm^{-1} (cellulose;xyloglucan) and of cross-peak at 1323;1650-1550 cm^{-1} (cellulose;pectin).*

Furthermore, from Figures 42 and 43 presented in Section 6.2.2., it can be seen that, in the synchronous spectra of the (unsulphonated) primary cell wall material, lignin indicated cross-peaks with both pectin and protein, at 1508;1643 cm^{-1} and 1508;1612 cm^{-1}, respectively (Figure 42). The analogous signals were absent in the asynchronous spectra (Figure 43). This indicated that lignin interacts with both pectin and protein in the primary cell wall material. The cross-peak at 1612;1643 cm^{-1} (protein;pectin) was found in the synchronous spectra of the primary cell wall material (Figure 42), while the corresponding asynchronous cross-peak appeared as very weak (Figure 43), indicating that protein and pectin also interact in the primary cell wall.

Based on the results from the dynamic 2D FTIR spectra of the primary cell wall material (see also Section 6.2.2) and literature data, a schematic picture of possible cross-linkages was suggested. See Figure 40. Here, a number of different intermolecular bonding in the primary cell wall was illustrated where cellulose and xyloglucan are linked by hydrogen bonding, while cellulose and pectin, xyloglucan and pectin, lignin and pectin, and lignin and protein are covalently bounded and where pectin and protein are linked by ionic bounding. The results point to the presence of a highly interconnected structure, suggesting the existence of an interpenetrating network structure in the primary cell wall of spruce wood.

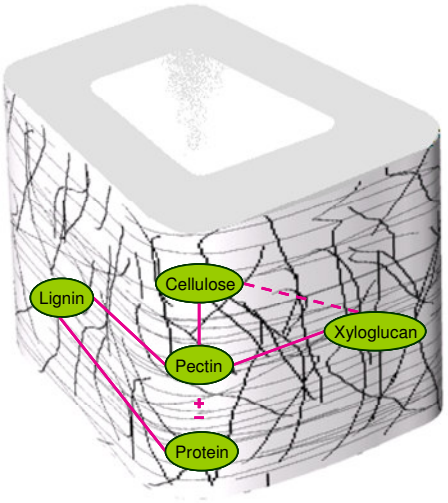

***Figure 40**: Illustration, showing the proposed ultrastructure of the primary cell wall of a softwood tracheid. The solid lines represent covalent bond, the broken line represents hydrogen bond and the ± represents ionic bond. The randomly oriented black lines represent cellulose microfibrils.*

6.2 *Effect of a low degree of sulphonation on the molecular interactions in the primary cell wall* – *PAPER III*

At low levels of sulphonation of softwood (0.1% to 0.4%, calculated as the weight of Na_2SO_3 on the oven dry weight of the chips), the primary cell wall is selectively affected. Here, a selective sulphonation of the lignin may occur, which may increase the lignin hydrophilicity and swelling, and consequently cause a weakening of the primary cell wall structure [2]. Also, a de-esterification of the pectin may cause a formation of a significant amount of new carboxylic groups (COO^-) and a high local charge concentration, which further may result in a selective fibre separation [4-6]. This results in a more energy efficient mechanical pulping process [7,8]. The reduction in electrical energy consumption for refining of chips with a low degree of sulphonation (0.11% wt.% Na_2SO_3), amounts to approximately 200 kWh/t, when compared to TMP refining at the same tensile index; the result from this study. At high levels of sulphonation (1% to 3% wt.% Na_2SO_3), the secondary cell wall is affected and the refining process requires even more energy than in conventional TMP, probably due to increased flexibility and compressibility of the fibres [4]. The low degree sulphonation process has, however, been shown to be extremely difficult to control. This is the reason why a better understanding of the mechanism may be a way of improving its applicability. Consequently, a low sulphonation reaction was carried out on spruce wood chips during an impregnation pre-treatment. The chips were first impregnated in water, according to a steam/cold liquor method, in order to ensure a uniform impregnation of the Na_2SO_3. The pulp, produced from these impregnated chips, displayed mechanical and optical properties similar to a TMP type of pulp, with an anticipated lower consumption of energy. Primary cell wall material was prepared from a first stage pulp obtained during these trials. The ultrastructural changes due to the low sulphonation reaction were examined using both dynamic FTIR spectroscopy and dynamic 2D FTIR spectroscopy.

6.2.1 *Load-bearing polymers in the sulphonated primary cell wall*

The dynamic in-phase FTIR spectra of the unsulphonated primary cell wall material and the sulphonated primary cell wall material (0.11% wt.% Na_2SO_3) are compared in Figure 41. The two materials had quite similar elastic responses. The same polymers appear as load-bearing in both the unsulphonated and sulphonated primary cell wall

materials. This illustrates that the ultrastructure of the sulphonated primary cell wall remained more or less unchanged from that of the native cell wall. However, some differences were observed for the pectin vibrations, at 1643 cm^{-1} (asymmetric stretching vibrations of the COO^- groups from the D-galacturonic acid units, (GalA)) [128], and for the protein vibrations, at 1612 cm^{-1} (N-H stretching vibrations of the primary amines) [128,129]. The xyloglucan absorption peak at 1597 cm^{-1} was observed for the unsulphonated primary cell wall material, but this was not at all obvious in the sulphonated primary cell wall material. The most significant difference between the two materials was that the lignin peak, occurring at 1276 cm^{-1} (C_{aryl}-O vibrations) [79,123,130], seemed to have disappeared in the spectra of the sulphonated material, indicating a change in lignin structure, due to the sulphonation.

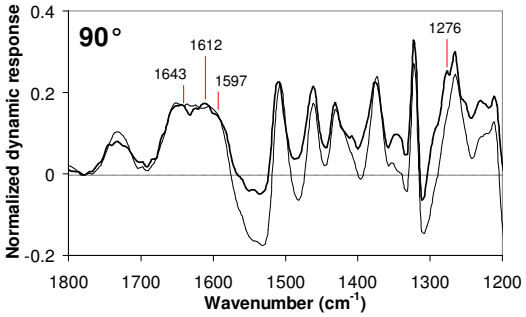

***Figure 41**: Dynamic in-phase FTIR spectra of sulphonated primary cell wall material (thin line) and unsulphonated primary cell wall material (thick line), recorded at a 90° polarisation, 60% RH and 30 °C.*

6.2.2 Interactions among polymers in the sulphonated primary cell wall

To obtain more information on any changes in the interactions between lignin;pectin, between lignin;protein as well as between protein;pectin, 2D correlation analyses were done. The synchronous and asynchronous 2D FTIR correlation spectra of the unsulphonated primary cell wall material, recorded at 60% RH in a 90° polarisation mode, are shown in Figures 42 and 43. The correlation spectra of the sulphonated primary cell wall material are illustrated in Figures 44 and 45.

As discussed above (see Figures 38 and 39 in Section 6.1.3), the synchronous and asynchronous 2D FTIR correlation spectra of the (unsulphonated) primary cell wall material show cross-correlations between cellulose;xyloglucan and cellulose;pectin.

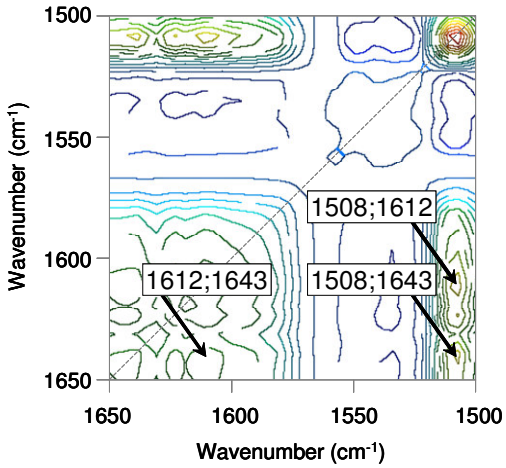

***Figure 42**: Synchronous 2D FTIR spectrum of unsulphonated primary cell wall material, recorded at a 90° polarisation, 60% RH and 30 °C, indicating a strong cross-peak at 1508;1643 cm^{-1} (lignin;pectin), a strong cross-peak at 1508;1612 cm^{-1} (lignin;protein) and a strong cross-peak at 1612;1643 cm^{-1} (protein;pectin).*

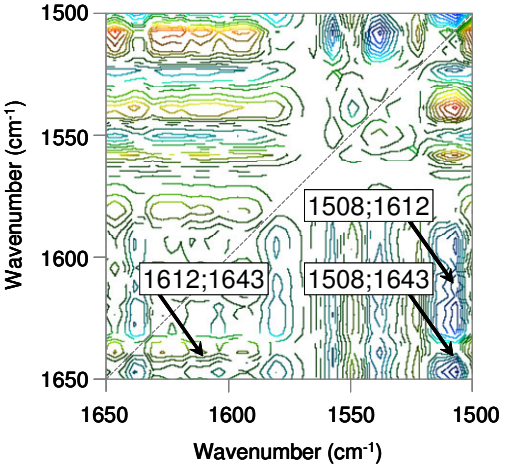

***Figure 43**: Asynchronous 2D FTIR spectrum of unsulphonated primary cell wall material, recorded at a 90° polarisation, 60% RH and 30 °C, indicating a weak cross-peak at 1508;1643 cm^{-1} (lignin;pectin), a weak cross-peak at 1508;1612 cm^{-1} (lignin;protein) and a weak cross-peak at 1612;1643 cm^{-1} (protein;pectin).*

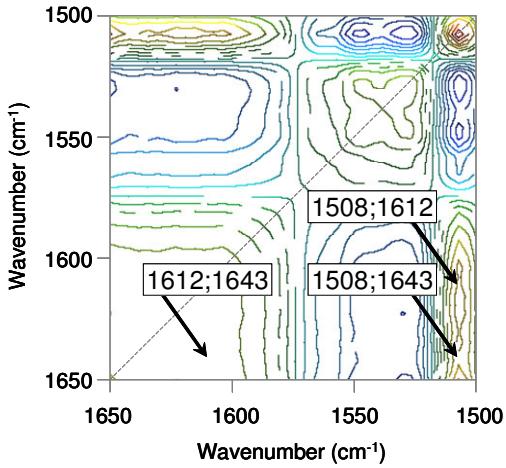

***Figure 44**: Synchronous 2D FTIR spectrum of sulphonated primary cell wall material, recorded at a 90° polarisation, 60% RH and 30 °C, indicating a strong cross-peak at 1508;1643 cm^{-1} (lignin;pectin), a strong cross-peak at 1508;1612 cm^{-1} (lignin;protein) and an absence of cross-peak at 1612;1643 cm^{-1} (protein;pectin).*

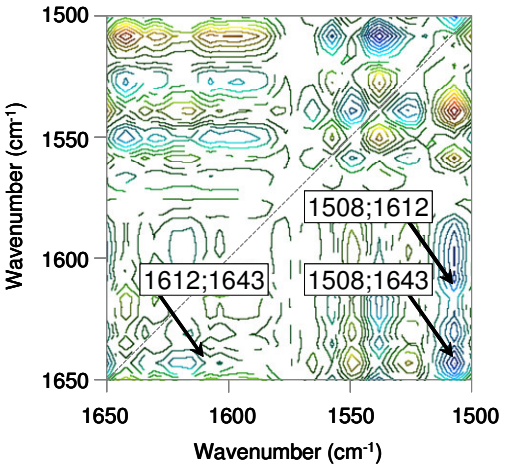

***Figure 45**: Asynchronous 2D FTIR spectrum of sulphonated primary cell wall material, recorded at a 90° polarisation, 60% RH and 30 °C, indicating a strong cross-peak at 1508;1643 cm^{-1} (lignin;pectin), a strong cross-peak at 1508;1612 cm^{-1} (lignin;protein) and a strong cross-peak at 1612;1643 cm^{-1} (protein;pectin).*

In the synchronous spectra of the unsulphonated material, lignin indicated cross-peaks with both pectin and protein, at 1508;1643 cm^{-1} and 1508:1612 cm^{-1}, respectively (Figure 42). The analogous signals were absent in the asynchronous spectra (Figure 43). This indicated that lignin interacts with both pectin and protein in the unsulphonated material. The cross-peak at 1612;1643 cm^{-1} (protein;pectin) was found in the synchronous spectra of the unsulphonated material (Figure 42), while the corresponding asynchronous cross-peak appeared as very weak (Figure 43), indicating that protein and pectin also interact in the primary cell wall.

For the sulphonated material, the lignin;pectin and lignin;protein cross-peaks were observed in the synchronous spectra (Figure 44), while the corresponding cross-peaks in the asynchronous spectra appeared as very strong (Figure 45). This means that the interactions of lignin with pectin and protein were significantly weakened in the material after the low degree sulphonation pre-treatment. The absence of the protein;pectin (1612;1643 cm^{-1}) cross-peak in the synchronous spectra and the presence of peaks in the asynchronous spectra, point to a destabilized association between protein and pectin after the low degree sulphonation reaction.

These results indicate that the low degree sulphonation (0.11% Na_2SO_3) has primarily altered the interactions of the lignin with other components in the primary cell wall. Based on viscoelastic measurements at different relative humidities, it was established that an increased softening of the primary cell wall occurs as a result of the sulphonation. It was suggested that this increased viscoelasticity, due to the breakdown of bonds between lignin;pectin and lignin;protein, could be recognised as the main reason for the lower consumption of energy achieved during the refining of such pulps, when compared to unsulphonated TMP.

6.3 *Orientation and interactions of the polymers in the secondary cell wall – PAPER IV*

The secondary cell wall of wood fibre plays an important role regarding the mechanical and physical properties of a whole fibre. The secondary cell wall is the constitution of three different cell wall layers, where the S_2 layer dominates. Its constitutive components are: cellulose, *O*-acetilgalactoglucomannan (glucomannan), arabino-4-*O*-methylglucuronoxylan (xylan) and lignin. The orientation of these polymers may, particularly, under moist conditions play an important role for the mechanical properties of wood and wood fibres. In order to better understand the interactions between these polymers, the orientation among the polymers was investigated using imaging FTIR microscopy in combination with a polariser.

6.3.1 *Orientation of polymers in the secondary cell*

Spectral signals related to absorptions from cellulose, glucomannan, xylan and lignin are found in the wavenumber range between 1800 cm^{-1} and 720 cm^{-1}. In Figure 46, in so-called orientational spectra, the positive signals indicate that their corresponding functional groups are arranged more parallel to the fibre axis, whereas the negative signals indicate that their corresponding functional groups are arranged more perpendicular to the fibre axis (cf. Equation(12)). The intensity of the signals indicate the degree of parallel and perpendicular orientations to the fibre axis for the corresponding functional groups, and consequently the polymers from which the functional groups originate.

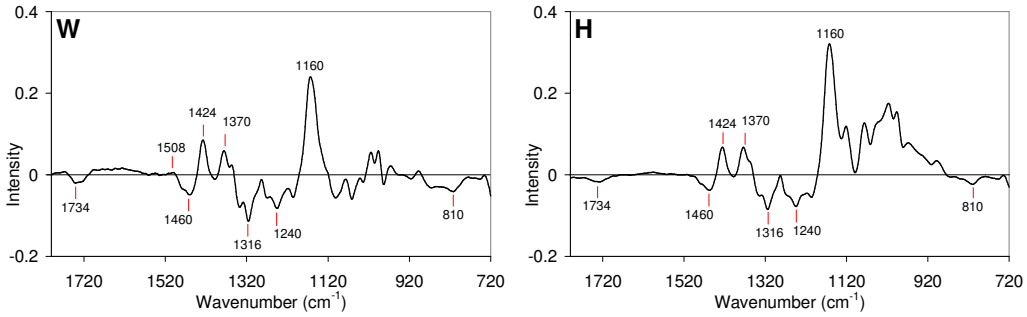

***Figure 46**: Average orientational spectra of wood fibres (W) and holocellulose fibres (H), respectively. In each spectra specific absorption peaks related to the different wood polymers are indicated; cellulose 1160 cm^{-1}, 1316 cm^{-1}, 1370 cm^{-1} and 1424 cm^{-1}, glucomannan 810 cm^{-1}, xylan 1734 cm^{-1}, 1460 cm^{-1} and 1240 cm^{-1} and lignin 1508 cm^{-1}.*

Here, two types of spruce fibres were presented: wood fibres (W) – fibres from the first stage of a TMP, in which the outer fibre wall layers were removed by mechanical action so that the S_2 layer was set free, and holocellulose fibres (H) – chemically delignified holocellulose fibres, which were analysed for comparison.

Three vibration peaks of cellulose, i.e. (a) the antisymmetric C–O–C bridge stretching vibration at 1160 cm^{-1}, (b) the C–H bending vibration at 1370 cm^{-1} and (c) the CH_2 symmetric bending vibration of the CH_2–OH group at 1424 cm^{-1}, are vibrations that are oriented parallel with the cellulose chain [72,92,131,132]. All of these peaks appeared as sharp positive signals in the average orientational spectra of the two fibres. This is in agreement with the general orientation of the cellulose in a near to parallel orientation to the fibre axis in the S_2 cell wall. This result is also in agreement with a negative cellulose vibration, i.e. the CH_2 wagging vibration found at 1316 cm^{-1} [67,92,131,132], which arise from a perpendicular vibration with respect to the cellulose backbone. A glucomannan absorption vibration caused by the equatorially aligned hydrogen at the C2 atom in the mannose residue, found at 810 cm^{-1} [67,131,132], appeared as a negative peak in the two orientational spectra. As this group is oriented orthogonal to the glucomannan backbone, this indicates that also the glucomannan was oriented more parallel to the fibre axis. This means that cellulose and glucomannan seems to be arranged parallel in respect to each other, as also previously stated [65,67]. For the xylan, a negative signal from the carbonyl group vibration, i.e. C=O stretching vibrations in the O=C–OH group of the glucuronic acid units (GlcA) at 1734 cm^{-1} [67,131-133], appeared with varying intensities in the two orientational spectra. It is reported that the carbonyl group have the transition moment at an angle of 54°44' to the polymer axis [131,133]. This was based on studies on oriented samples of the 4-*O*-methyl-D-glucuronoxylan from white birch using polarised IR light. This fact could explain the rather low intensity of this negative signal. Two other xylan signals assigned as being perpendicular to the chain axis, i.e. (a) the CH_2 symmetric bending on the xylose ring at 1460 cm^{-1} and (b) the C–O stretching in the O=C–O group at 1240 cm^{-1} [131-133], also appeared as negative in the orientational spectra calculated. The xylan CH_2 group in the xylose unit, which is attached directly to the pyranose ring [133], has a different vibrational energy compared to the cellulose CH_2 group, which is from the hydroxymethyl group (–CH_2–OH) of the glucose unit. This xylan vibration has no overlapping contribution from cellulose vibration and gives thus a possibility to

selectively analyse the orientation of the xylan chain. This xylan vibration has earlier been reported as associated to a perpendicular vibration to the xylan chain axis [133]. Based on the presence of the three negative xylan vibrations, at 1734 cm^{-1}, 1460 cm^{-1} and 1240 cm^{-1}, it may be suggested that the xylan has also a more parallel orientation with respect to the fibre axis. This further means that all of the carbohydrate wood polymers, i.e. the cellulose, glucomannan and xylan, seem to be oriented more or less parallel with respect to the fibre axis. For the wood fibre, a lignin vibration, i.e. the C=C aromatic ring vibrations at 1508 cm^{-1} [79,131,132], showed a weak positive signal indicating the presence of some degree of parallel orientation of the lignin to the fibre axis, which means that the lignin should not be isotropically arranged in the cell wall, a fact also suggested earlier [79].

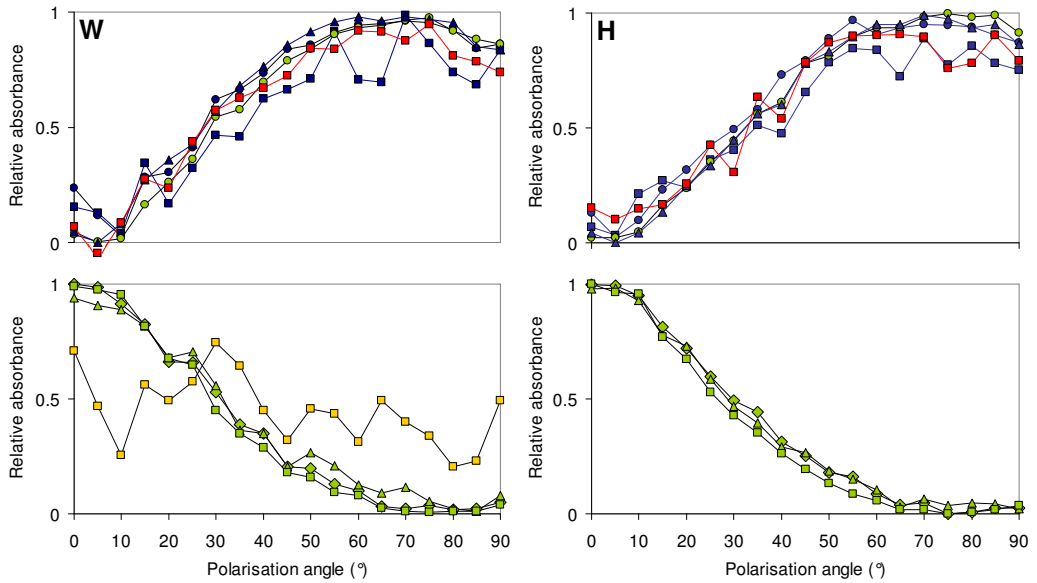

***Figure 47**: Relative absorbance of IR specific absorption wavenumber versus polarisation angle for the wood polymers in a wood fibre (W) and a holocellulose fibre (H). Cellulose (green) (■) C–O–C stretching at 1160 cm^{-1}, (●) CH_2 wagging at 1316 cm^{-1}, (▲) C–H bending at 1370 cm^{-1} and (♦) C–OH bending at 1424 cm^{-1}. Glucomannan (red) (■) equatorially aligned H vibration at 810 cm^{-1}. Xylan (blue) (■) C=O stretching at 1734 cm^{-1}, (●) CH_2 bending at 1460 cm^{-1} and (▲) C–O stretching at 1240 cm^{-1}. Lignin (yellow) (■) C=C aromatic vibration at 1508 cm^{-1}.*

Figure 47 illustrates how the relative absorbances (based on Equation (13)) for the different signals depend on the polarisation angle for the fibres studied. In this way, the angular dependence of the different vibrations may be more easily compared. It is obvious that the three cellulose signals, with high absorption at the low polarisation

angle, followed each other very nicely. The fourth cellulose signal, the perpendicular vibration at 1316 cm^{-1}, showed its highest intensity at the very high degrees of polarisation. It is therefore obvious that the cellulose is oriented more or less parallel to the fibre axis. Mathematically, it can be estimated that the cellulose chains in both the wood fibre and holocellulose fibre were oriented at fibril angles lower than 5°. For the glucomannan, the signal from the perpendicular hydrogen vibration at 810 cm^{-1} increased with the increase in the degree of polarisation. In most cases, the angular dependence was very well matching that of the cellulose 1316 cm^{-1} signal indicating that the glucomannan must be considered to be aligned parallel to the cellulose chains. The variations of this vibration can be explained as due to the rather low intensity of this absorption. All the three xylan signals followed, in most cases, very nicely the same angular dependence as the negative vibrations assigned to the cellulose and glucomannan, respectively. The good agreement between the angular dependence of the signals from the xylan and those of glucomannan and cellulose suggests that also the xylan may be orientated parallel with the cellulose and the glucomannan. The lignin vibration showed no defined trend with regard to the polarisation angle. Somewhat higher absorption was observed for the 0° compared to 90° polarisation. The angular dependence of the absorption points to a main orientation of 30° to 40° to the fibre axis. It is likely to conclude that the lignin is showing a low degree of the parallel orientation in the fibres. Still it can not be stated that the lignin shows an isotropic arrangement in the cell wall of softwood fibres.

Recently, some additional studies were done, in our lab, on the orientation of the cellulose, glucomannan, xylan and lignin in wood fibres of various origins using imaging FTIR microscopy [74-76]. The results from these studies support the findings from this study (see Section 3.2), and it can be concluded that the strongly oriented assembly of the cellulose microfibrils/hemicelluloses may determine the orientation pattern of some part of the lignin in the secondary cell wall, which seams to be in parallel to the orientation of the cellulose microfibrils and the fibre axis. Some variation in the orientation of the cellulose as well as the hemicelluloses can be explained by the cellulose/hemicelluloses undulating structure in the S_2 layer [134]. This particular undulating structure and the limited spatial size of the pores created with this structure, with an aspect ratio larger than 1, can be an explanation for the observed orientational pattern of the lignin [76].

6.3.2 *Interactions among polymers in the secondary cell wall*

Based on the results from imaging FTIR spectra, it is concluded that both the hemicelluloses in softwood fibres, i.e. glucomannan and xylan, show a predominant orientation and that they are arranged in parallel with the cellulose microfibrils within the S_2 cell wall. This and literature data (see Section 3.2) may strongly support the presence of an intimate arrangement between the polysaccharides. Most likely, after that the cellulose microfibrils have been synthesised on the exposure of the hemicelluloses gel [55], the glucomannan deposition may be initiated on the microfibrils. This may be a cause for a parallel orientation of the two polysaccharides in respect to each other. This suggestion that the glucomannan of the two possible hemicelluloses is firstly connected to the cellulose microfibrils can be supported by the structure of the secondary cell wall based on mechanical interactions as presented by Salmén and Olsson [11], and the results from the dynamic interactions studies made by Åkerholm and Salmén where a closer association of the glucomannan than the xylan to the cellulose was seen in spruce wood [67] (cf. Figure 14). One could say that these two polysaccharides make a closely associated template in the S_2 cell wall, which strongly may influence the arrangement of the additional components. Here, the observed parallel orientation of xylan, with respect to both cellulose and glucomannan in the S_2 layer, may support an intimate and persistent arrangement between the polysaccharides. Further, it is more likely to conclude that the xylan is more interacting with accessible glucomannan than with the cellulose itself. Lower intensities of the orientational signals of the hemicelluloses than of the cellulose were observed. From this, it could be suggested a somewhat lower degree of parallel orientation of the hemicelluloses than of the cellulose microfibrils, and that the hemicelluloses may cross-link the cellulose microfibrils. A number of authors suggest different functions of the hemicelluloses in the secondary cell wall of a wood fibre; (a) the hemicelluloses are integrated into the structure of the cellulose microfibrils during aggregation and adsorbed onto the surface of the cellulose microfibrils, but also provide various branches for association with specific lignin precursors [54]; (b) the hemicelluloses determine the aggregation pattern of the cellulose microfibrils due to that the deposition of these polysaccharides occur at the same time, and they together provide the pattern for assembly of the lignin under the lignification process, which occurs after the completed deposition of the polysaccharides [55]. For the lignin, some degree of the parallel orientation is indicated but a much more random arrangement

than that of the other wood polymers seems at hand. This orientation of lignin can be explained due to a presence of the prior and distinct mostly parallel arranged template made by the three polysaccharides, and also of the potential networks of the hemicelluloses. Since the lignin is deposited after the biosynthesis of cellulose and hemicelluloses during the process of lignification of the S_2 layer [55], it is possible to assume that lignin fills up the interspace left, most probably interacting with xylan. This can be supported by results from the study made by Salmén et al. on wood fibres from different origins where some part of lignin shows a parallel orientation to the fibre axis that might be guided by the undulated cellulose microfibrils/hemicelluloses structure of the secondary cell wall [76].

6.4 *Interactions between model components in the cellulose/hemicellulose biocomposite films* – *PAPERS V and VI*

Production of environmentally friendly packaging materials, based on renewable polysaccharides, is increasingly demanded. Nanocomposite films made of non-food plant-derived hemicelluloses (arabinoxylan, AX and galactoglucomannan, GGM) and microbial or wood-derived celluloses (bacterial cellulose, BC and microfibrillated cellulose, MFC) may provide a potential alternative for future biobased packaging materials. The mechanical strength of hemicellulose based films has to be improved for this targeted application. One possibility to enhance the performance of hemicellulose films is by reinforcing them with various nanoscale celluloses. In order to improve the mechanical performance of the nanocomposite films, their mechanical properties have been examined using DMA and the interactions between the components were studied.

6.4.1 *Mechanical properties of the biocomposite films*

Table 2*: Average values of Young's modulus (E), stress at break (σ_b) and strain at break (ε_b) of: a) rAX, b) rDAX and c) GGM films studied. Values in brackets are standard deviations (see also Table 1, Section 5.1.5).*

Code	*Young's modulus, E (GPa)*	*Stress at break, σ_b (MPa)*	*Strain at break, ε_b (%)*
a)			
rAX	2.5 ±0.4	58 (11)	8.1 (3.3)
rAX:5BC	2.7 ±0.3	68 (11)	8.1 (3.1)
rAX:15BC	3.2 ±0.5	53 (7)	3.3 (0.6)
b)			
rDAX	2.2 ±0.2	32 (3)	2.1 (0.3)
rDAX:5BC	3.1 ±0.4	46 (5)	2.8 (1.0)
rDAX:15BC	3.7 ±0.5	49 (8)	2.8 (1.3)
c)			
GGM/40gly	0.3 ±0.1	6.0 (0.7)	4.9 (0.8)
GGM/30gly	0.4 ±0.1	7.3 (0.5)	3.3 (0.7)
GGM/20gly	1.2 ±0.1	13.1 (0.6)	1.5 (0.2)
GGM:15MFC/40gly	1.1 ±0.3	15.2 (2.2)	2.6 (0.6)
GGM:15MFC/30gly	1.8 ±0.2	22.7 (0.5)	2.1 (0.3)
GGM:15MFC/20gly	3.1 ±0.4	31.9 (5.8)	1.6 (0.2)
GGM:15MFC/10gly	3.5 ±0.3	34.4 (8.9)	1.3 (0.7)

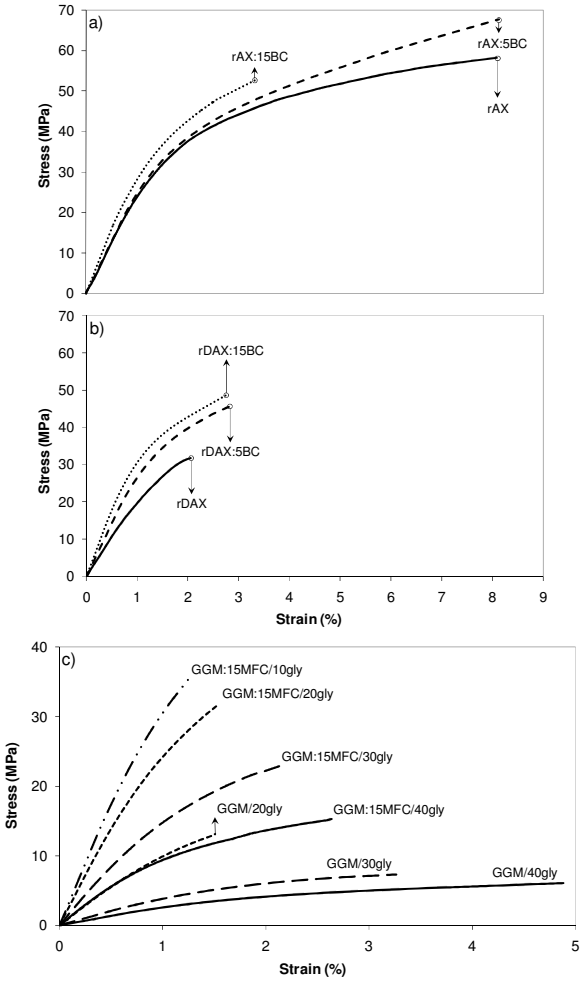

***Figure 48**: Stress-strain curves of composite films recorded at 50% RH, 30 °C; a) rAX, b) rDAX and c) GGM.*

Figures 48a and 48b show average stress-strain curves of the rye arabinoxylan films (unmodified, rAX - Ara/Xyl ratio 0.50, and enzymatically modified, rDAX - Ara/Xyl ratio 0.16), as neat and reinforced with BC (5% and 15% w/w), tested at 50% RH, 30 °C. The reinforcement with BC made the AX films stronger (higher stress at break, σ_b) and stiffer (higher Young's modulus, E); the higher the amount of BC the higher the strength and stiffness of the films. Also, elongation (higher strain at break, ε_b) of the composite films seemed to be improved, but one would expect that the elongation will decrease with the reinforcement. Debranching of the hemicellulose decreased the strength and elongation and improved the stiffness of corresponding films (see Table 2). The deviations seen (for the rAX:15BC film with regard to σ_b, ε_b and reinforcement, and the rDAX film with regard to E and debranching) were most likely due to the morphology of the films and the occurred agglomeration; for more details see PAPER V. Figure 48c shows average stress-strain curves of the spruce

galactoglucomannan films, both pure and reinforced with MFC (15% w/w), with different amounts of glycerol added (i.e. 40%, 30%, 20% and 10%, w/w of GGM), tested at 50% RH, 30 °C. The reinforcement with MFC made the GGM films stronger, stiffer and more brittle. The pure GGM films as well as the composite films with MFC became successively stronger, stiffer and more brittle with the lower amount of plasticiser added (cf. Table 2).

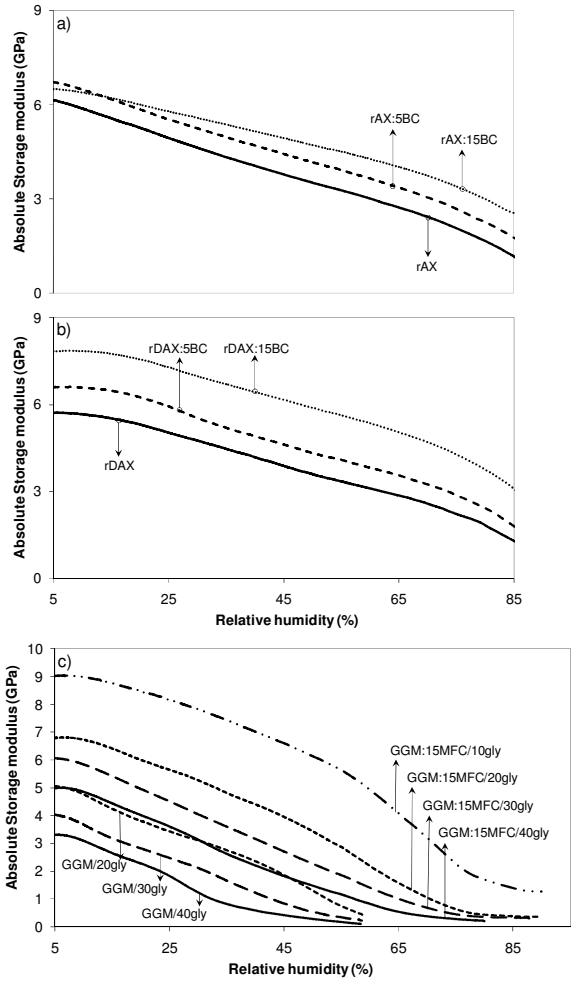

***Figure 49**: Absolute storage modulus of composite films as a function of relative humidity, showing their stiffness; a) rAX, b) rDAX and c) GGM.*

The moisture effects on stiffness of the AX films are shown in Figures 49a and 49b. With increasing amounts of BC, the films increased in stiffness. All the composite films made from the debranched xylan were stiffer than their corresponding films made from unmodified xylan. The rDAX:15BC film appeared as the stiffest and the rAX film as the least stiff. Both the reinforcement and debranching increased the stiffness (higher storage modulus, E'). Note the lower stiffness at the lower RHs for

the rAX:15BC film (Figure 49a) that can be related to the morphology of this film mentioned above. The moisture effects on stiffness of the GGM films are shown in Figure 49c. The GGM/40gly film showed the lowest stiffness of all the films studied. A successive lowering of the amount of added plasticiser caused an increase in the stiffness of the corresponding films. For the GGM films with reinforcing MFC, the stiffness successively increased as the amount of the plasticiser was decreased. Both the reinforcement and lower amount of glycerol increased the stiffness.

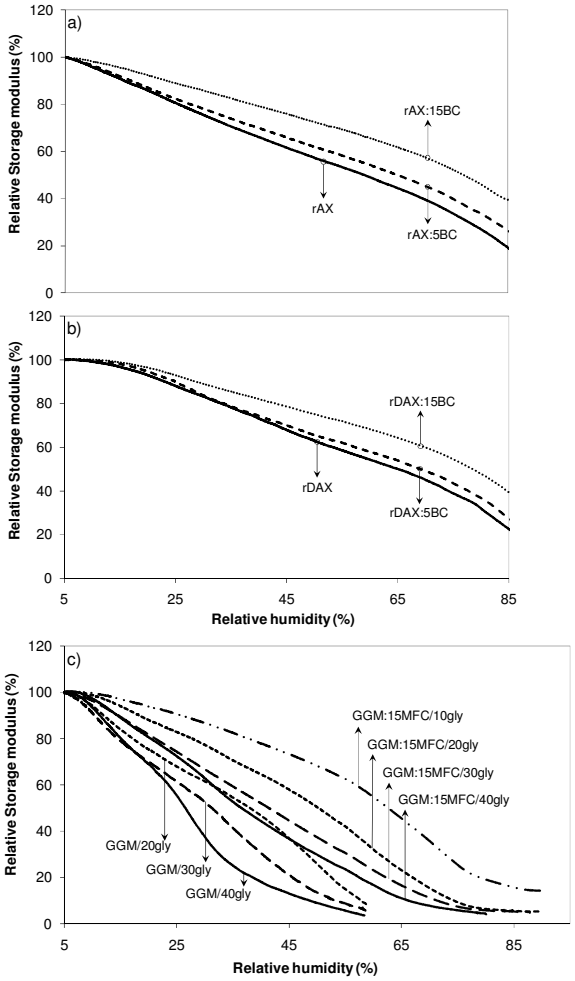

***Figure 50**: Relative storage modulus of composite films as a function of relative humidity, showing their softening ability; a) rAX, b) rDAX and c) GGM.*

In Figures 50a and 50b, the relative moduli, i.e. softening behaviour, are compared for the rAX and the rDAX films, respectively. Moisture, clearly, reacted as a plasticizer for the polysaccharides, which was evident from the decrease in storage modulus, E'. The film made from the pure arabinoxylan, rAX, as well as its composite films (i.e. rAX:5BC and rAX:15BC) showed a slightly higher degree of softening as compared

to the corresponding films made from debranched arabinoxylan (i.e. rDAX, rDAX:5BC and rDAX:15BC). The higher the amount of BC, the lower was the degree of softening. Both the reinforcement and debranching decreased the softening. In Figure 49c, the relative moduli are compared for the neat and composite spruce GGM films, from which the softening behaviour of the films was deduced. The GGM/40gly film showed the highest relative degree of softening at relatively low RHs. The composite films with MFC with the same amount of glycerol (40%) retained the stiffness to higher RHs than the pure GGM/40gly film. The clear effect of the plasticiser is also seen from Figure 50c. The lower the amount of plasticiser, the higher the RH at which softening occurred of both the neat and composite films. Both the moisture and higher amount of glycerol increased the softening, while the reinforcement decreased the softening.

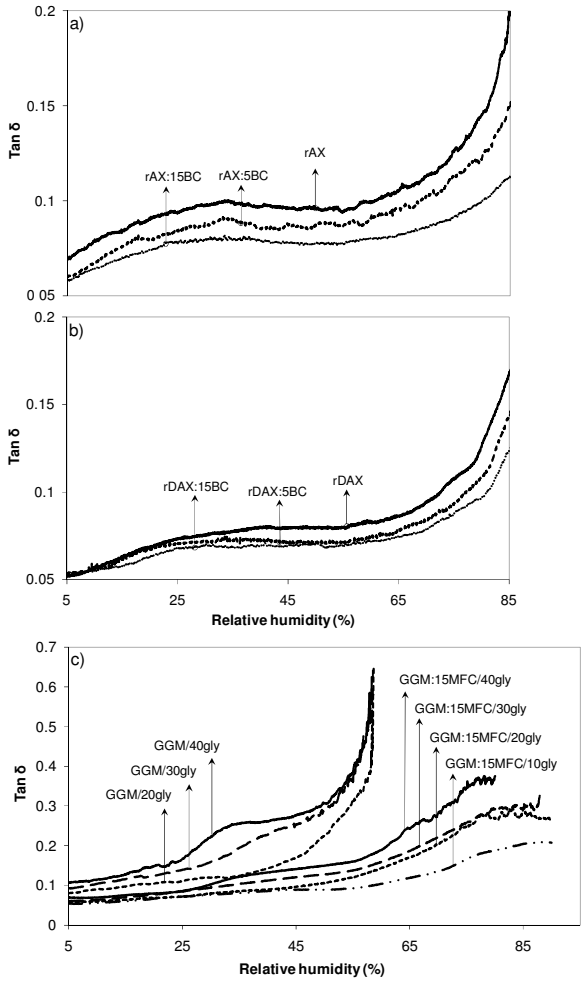

***Figure 51**: Tan δ of composite films as a function of relative humidity, showing their damping behaviour; a) rAX, b) rDAX and c) GGM.*

The loss tangent (tan δ) for the AX films increased, as expected, with an increasing RH (Figures 51a and 51b). Two transition points could be noted; a secondary transition around 20% RH and the main transition [135] at around 80% RH. The secondary transition was more apparent for the films (neat and composites) made from the unmodified arabinoxylan, rAX. The main transition at 80% RH was attributed to the moisture-induced glass transition of the arabinoxylan backbone [117,136,137]. Figures 51a and 51b also illustrate that the composite films showed a lower damping factor than the pure films; the higher the amount of the BC the lower the damping factor. Both the reinforcement and debranching lower the damping, and the materials appeared as less viscous and more elastic. The loss tangent for the GGM films increased, as expected, with an increasing RH (Figure 51c). The lowest damping was seen for the composite film with lowest amount of glycerol (GGM:15MFC/10gly). The damping effect of the composite films successively increased with the higher amount of plasticiser. The pure spruce GGM films showed the highest damping factor, where the damping effect increased with the higher amount of glycerol added. Both the reinforcement and the less amount of glycerol lower the damping.

To summarise the mechanical studies of the nanocomposite films; the stiffness was increased by the reinforcement, debranching and decreased by addition of glycerol. Further, the strength was increased by the reinforcement but decreased by the debranching and addition of glycerol, and, finally, the elongation, softening and damping were decreased by the reinforcement, debranching and increased by addition of glycerol. With other words, the reinforcement made stronger, more elastic films, more brittle and resistant to moisture. In contrary, the addition of glycerol made weaker, more viscous films, less brittle and resistant to moisture. The debranching made stiffer but weaker films, more elastic, more brittle and more resistant to moisture.

6.4.2 Interactions among polymers in the biocomposite films

From the results on the interactions between polymers in the primary and secondary cell walls of spruce fibres (PAPERS I-IV), it was evident that cellulose and hemicellulose strongly interact through intermolecular hydrogen bonding in their unsubstituted regions of the backbones. This strong affinity between these

polysaccharides was mimicked when preparing nanocomposite films, such as AX:BC and GGM:MFC films. Here, the chemical structure of hemicelluloses molecules (i.e. degree of substitution as well as its distribution) plays a crucial role. The interactions between constituent components in the films were affected by the debranching of the side groups (i.e. arabinose) and addition of plasticiser (i.e. glycerol). This was seen in the changes in viscoelastic properties of the films.

The effect of debranching on the interactions may be summarised: A higher amount of substituents will prevent intermolecular hydrogen bonding between xylan backbones and result in higher flexibility of the molecules [138]. When the arabinose side units are removed, a crystallisation occurs (~20%, see PAPER V), due to an increased ability of the unsubstituted regions of a xylan backbone to form stable insoluble inter-chain aggregates. Some previous studies have shown that only the backbone residues of different xylans take part in the crystallisation [133] and that xylan chains show an ability to associate with each other and crystallise when the arabinose substituents are removed [14,139,140]. The degree of substitution of a xylan molecule determines also its ability to bond to cellulose. The higher the degree of substitution of side chains the lower is its bonding ability to cellulose, while molecules with fewer side chains bind more tightly to cellulose [31]. This may explain the higher stiffness and brittleness for the AX:BC composite films made with modified arabinoxylan, rDAX, having fewer arabinose units. When discussing the degree of solubility of xylans, the difference between the two types of xylan (i.e. rAX and rDAX) can also be related to the degree of substitution. It was found that the substitution of a xylan backbone increases its solubility, mainly by preventing intermolecular hydrogen bonding [21,28], and by creating more free volume of the polymer molecule; the higher the degree of the substitution the higher the water solubility [14,31]. This may result in an increased hydration and be seen as a clear plasticizing effect. The lower damping seen for the rDAX compared to the rAX film can be a result of the occurred crystallisation, after debranching of the arabinose substituents [141]. A lower damping factor was also seen when reinforcing BC was introduced; the higher the amount of the BC the lower the damping factor, so the material behaved as less viscous and more elastic. Apart from the lowering of the damping factor due to the lower content of the xylan, also the possible interactions between cellulose and xylan might limit the moisture-induced mobility of the arabinoxylan chains [31].

The effect of plasticisation on the interactions may be summarised: Both the plasticisation and moisture increased the softening by preventing the intermolecular hydrogen bonding between GGM backbones, providing a higher mobility of the polymer chains and a higher free volume. Also, the accumulation of glycerol on the interface of GGM and MFC could be the reason for the decrease of the reinforcement effect, by preventing the load transfer between the two components in the composite films. For comparison, the strength of the unplasticised AX films increased when BC was added. A clear increase of the strength, due to an introduced cellulose reinforcement to unplasticised hemicellulose films, was already seen in some other studies [142,143]. A higher amount of plasticiser will result in higher flexibility of the molecule, i.e. higher damping, so the material appeared as less elastic and more viscous.

In conclusion, the debranching and plasticisation showed an opposite effect on the interactions between the hemicellulose molecules and between the hemicellulose and cellulose molecules.

7 CONCLUSIONS AND FUTURE ASPECTS

Strong interactions between different wood polymers in softwood fibres and cellulose/hemicellulose biocomposites were here demonstrated.

(a) The studies using dynamic FTIR and dynamic 2D FTIR spectroscopies of the primary and sulphonated primary cell wall materials, demonstrated that:

- The cellulose in the primary cell wall material was the main load-bearing polymer. The load-bearing ability of the lignin in the primary cell wall material was much greater than of the lignin in the secondary cell wall. To a certain extent, all the polymers in the primary cell wall took part in the stress transfer.
- The dominating crystalline cellulose in the primary cell wall was the cellulose Iβ allomorph indicating that the cellulose microfibrils are formed in a more stress-free environment than those in the S_2 cell wall.
- *Strong interactions among the cellulose, xyloglucan and pectin as well as among the lignin, protein and pectin in the primary cell wall were suggested.* This suggested the presence of a highly interconnected structure and the probable existence of an interpenetrating network structure in the primary cell wall of spruce wood fibres.
- The low degree sulphonation reaction caused fractures in the range between the primary cell wall and the middle lamella of spruce chips. *The weakening of the interactions between the lignin;pectin and the lignin;protein as well as between the pectin;protein were suggested to be the cause*. This resulted in an increased softening of the primary cell wall material, which could be the primary reason behind the energy efficiency of this refining process.

If taking the advantage of this unique ultrastructure of the primary cell wall, there might be a good possibility of reducing the energy demand when refining spruce wood chips, by utilising treatments that would give a similar softening of the primary cell wall, such as that achieved by a low degree of sulphonation pre-treatment. Such energy savings might be achieved by applying other chemical and/or enzymatic treatments that show selective affinities to the components in the primary cell wall.

(b) From the study using imaging FTIR microscopy of the secondary S_2 cell wall of spruce fibres, it could be concluded that:

- The hemicelluloses, glucomannan and xylan, showed a predominant orientation, i.e. parallel with the cellulose microfibrils and more or less in parallel with the longitudinal axis of the fibre. This means that all of these components will show a clear anisotropic behaviour in a mechanical sense.
- The lignin showed a low degree of parallel orientation to the orientation of the polysaccharides, but no isotropic arrangement. Due to the successive and ordered biosynthesis of the polymers in wood fibres, this degree of parallel orientation of the lignin could be a result of the polysaccharides template arranged in the secondary S_2 cell wall prior the lignification process.
- *Strong interactions between cellulose and glucomannan as well as between xylan and lignin were suggested, but also strong interactions between the two hemicelluloses.*

To additionally improve the current knowledge on the orientation and interactions of the polymers in wood fibres, the fibres from other origins could be investigated and compared.

(c) From the results of the study using DMA on nanocomposite films of pure (rAX) and debranched (rDAX) rye arabinoxylan reinforced with bacterial cellulose (BC) and spruce galactoglucomannan (GGM) reinforced with spruce/pine microfibrillated cellulose (MFC), it could be concluded that:

- Reinforcement with BC and MFC increased the stiffness and strength but decreased the elongation, softening and damping of the films.
- Debranching of arabinose residues from arabinoxylan molecules increased the stiffness but decreased the strength, elongation, softening and damping of the films.
- Plasticisation of GGM with glycerol increased the elongation, softening and damping but decreased the stiffness and strength of the films.
- By reinforcing of the hemicellulose films with BC or MFC, *intramolecular hydrogen bonding might be created between the cellulose molecules and the unsubstituted areas of the backbones of the hemicellulose molecules.*

- Debranching and plasticisation showed opposite effects on the interactions between the hemicellulose molecules and between the hemicellulose and cellulose molecules; *the lower degree of substitution and the lower amount of glycerol added, the larger occurrence of intermolecular hydrogen bonding*.

For future studies, it could be interesting to perform dynamic FTIR measurements on these cellulose/hemicellulose biocomposite films. When designing biocomposite films based on hemicellulose reinforced with nanocellulose, it could be of interest to prepare a matrix phase from more than one hemicellulose, due to a fact that in structures of nature the matrix phase usually consists of more than one hemicellulose.

8 ACKNOWLEDGEMENTS

The work on the primary cell wall was partly carried out within the framework of the Wood Ultrastructure Research Center (WURC) in Uppsala, financed by VINNOVA, the Nordic pulp and paper industry and SLU (PAPERS I-III). The work on the biocomposites was carried out within the BioPack project financed by FORMAS through the WoodWisdom-Net program and supported by the Wallenberg Wood Science Center (WWSC), a cooperation centre between KTH and Chalmers (PAPERS V and VI). The study, itself, was carried out at INNVENTIA AB. I wish to express my sincere gratitude to all of these.

I would especially like to thank my supervisor, Associate Professor Lennart Salmén, for his support, guidance and genuine engagement during this work. My supervisors, Professor Lars Wågberg (KTH, licentiate part) and Professor Paul Gatenholm (Chalmers, doctoral part), are also acknowledged for valuable comments on this thesis.

I would also like to express my gratitude to Dr. Margaretha Åkerholm for her invaluable advice concerning the dynamic FTIR spectroscopy. I am indebted to Mr. Anders Mårtensson (Chalmers) and Ms. Joanna Hornatowska for kindly working on the SEM images. I would like to thank Mr. Lars-Åke Hammar for preparing the primary cell wall material, the sulphonated primary cell wall material as well as the wood fibres (W); Ms. Lisa Klockare for preparing the holocellulose fibres (H); Ms. Susanna Heikkinen (University of Helsinki) for help with the rDAX preparation; Professor Stefan Willför (Åbo Akademi) for providing the GGM; Mr. Mikael Ankefors for providing the MFC; and Ms. Åsa Blademo for performing homogenisation of the cellulose/hemicellulose mixtures. I would sincerely like to acknowledge Dr. Tomas Larsson for carrying out the NMR measurements.

I would also like to thank all my colleagues at INNVENTIA AB for their kindness and all their help. I would like to make special mention of Ms. Anne-Mari Olsson for her help with DMA and endless patience.

Finally, I would like to express my deepest gratitude to my parents for giving me such a good start in life, my two sisters for their exceptional support, and my Boris for all the love, understanding and encouragement he has given me during this time.

9 REFERENCES

(1) Salmén, L., Petterson, B. 1995 The primary wall; Important for fibre separation in mechanical pulp. *Cellulose Chemistry and Technology* 29:331-337.

(2) Westermark, U., Samuelsson, B., Simonson, R., Pihl, R. 1987 Investigation of selective sulfonation of wood chips. Part 5. Thermomechanical pulping with low addition of sulfite. *Nordic Pulp & Paper Research Journal* 2(4):146-151.

(3) Peng, F., Ferritsius, R., Ängsås, U. 2003 Mechanical pulping with pectinase pretreatment of wood chips. *2003 International Mechanical Pulping Conference*, Cape Town pp.335-340.

(4) Konn, J., Vähäsalo, L., Pranovich, A., Holmbom, B. 2006 De-esterification and Sulfonation in CTMP: Effects on Pulp and Paper Properties. *Holzforschung* 60(4):355-364.

(5) Konn, J., Pranovich, A., Holmbom, B. 2006 Dissolution of fibre material in alkaline pre-treatment and refining of såruce CTMP. *Holzforschung* 60(1):32-39.

(6) Konn, J., Holmbom, B., Nickull, O. 2002 Chemical Reactions in Chemimechanical Pulping: Material Balances of Wood Components in a CTMP Process. *Journal of Pulp and Paper Science* 28(12):395-399.

(7) Axelson, P., Simonson, R. 1982 Thermomechanical pulping with low addition of sulfite. Part 1. Effects of mild sulfite treatment of spruce chips prior to defibration. *Svensk Papperstidning* 85(15):R132-139.

(8) Axelson, P., Simonson, R. 1983 Thermomechanical pulping with low addition of sulfite. Part 4. A mill scale trial. *Svensk Papperstidning* 86(15):R149-R151.

(9) Noda, I. 1994 Dynamic Two-Dimensional IR Spectroscopy. *Analytical Chemistry* 66(21):1065-1075.

(10) Plomion, C., Laprovost, G., Stokes, A. 2001 Wood Formation in Trees. *Plant and cell physiology* 127:1513-1523.

(11) Salmén, L., Olsson, A.-M. 1998 Interaction Between Hemicelluloses, Lignin and Cellulose: Structure-Property Relationships. *Journal of Pulp and Paper Science* 24(3):99-103.

(12) Nisperos-Carriedo, M. O. 1994 Edible coatings and films based on polysaccharides. In: *Edible Coatings and Films to Improve Food Quality*

Krochta, J. M., Baldwin, E. A., Nisperos-Carriedo, M. O., Eds., Technomic Publishing Company, Lancaster 305-336.

(13) Gröndal, M., Eriksson, L., Gatenholm, P. 2004 Material Properties of Plasticized Hardwood Xylans for Potential Application of Oxygen Barrier Films. *Biomacromolecules* 5:1528-1535.

(14) Höije, A., Sternemalm, E., Heikkinen, S., Tenkanen, M., Gatenholm, P. 2008 Material Properties of Films from Enzymatically Tailored Arabinoxylans. *Biomacromolecules* 9:2042-2047.

(15) Mikkonen, S. K., Heikkinen, S., Soovre, A., Peura, M., Serimaa, R., Talja, A. R., Helén, H., Hyvönen, L., Tenkanen, M. 2009 Films from oat spelt arabinoxylan plasticized with glycerol and sorbitol. *Journal of Applied Polymer Science* 114:457-466.

(16) Sjöström, E. 1981 *Wood chemistry. Fundamentals and applications* Academic Press Inc., Orlando 223.

(17) Atalla, R. H., D.L.VanderHart 1984 Native Cellulose: A Composite of Two Distinct Crystalline Forms. *Science* 223:283-285.

(18) Debzi, E. M., Chanzy, H., Sugiyama, J., Tekely, P., Excoffier, G. 1991 The Iα/Iβ transformation of highly crystalline cellulose by annealing in various mediums. *Macromolecules* 24:6816-6822.

(19) O´Sullivan, A. C. 1997 Cellulose: The Structure Slowly Unravels. *Cellulose* 4:173-207.

(20) Wangaard, F. F. 1970 Mechanisms of cell-wall growth in secondary xylem. *Wood and Fiber* 2(3):188-195.

(21) Bacic, A., Harris, P. J., Stone, B. A. 1988 Structure and Function of Plant Cell Walls. In: *The Biochemistry of Plants* Preiss, J., Ed., Academic Press, Inc., New York 297-371.

(22) Kataoka, Y., Kondo, T. 1998 FT-IR Microscopic Analysis of Changing Cellulose Crystalline Structure during Wood Cell Wall Formation. *Macromolecules* 31:760-764.

(23) Fengel, D. 1970 Ultrastructural Behaviour of Cell Wall Polysaccharides. *Tappi* 53(3):497-503.

(24) Kerr, A. J., Goring, D. A. I. 1975 The ultrastructural arrangement of the wood cell wall. *Cellulose Chemistry and Technology* 9(6):563-573.

(25) Kollmann, F. F. P., Wilfred A. Côté, J. 1968 *Principles of Wood Science and Technology I* Springer-Verlag New York Inc., New York 1-54.

(26) Fengel, D., Wegener, G. 1984 *Wood: Chemistry, Ultrastructure, Reactions* Walter de Gruyter, Berlin, New York 613.

(27) Atalla, R. H., Hackney, J. M., Uhlin, I., Thompson, N. S. 1993 Hemicelluloses as Structure Regulators in the Aggregation of Native Cellulose. *International Journal of Biological Macromolecules* 15:109-112.

(28) Carpita, N., McCann, M. 2000 The Cell Wall. In: *Biochemistry & Molecular Biology of Plants* Buchanan, B., Gruissem, W., Jones, R., Eds., American Society of Plant Physiologists, Rockville 52-108.

(29) Reid, J. S. G. 1997 Carbohydrate Metabolism: Structural Carbohydrates. In: *Plant Biochemistry* Dey, P. M., Harborne, J. B., Eds., Academic Press, London 205-236.

(30) York, W. S., Darvill, A. G., Albersheim, P. 1984 Inhibition of 2,4-dichlorophenoxyacetic acid-stimulated elongation of pea stem segments by a xyloglucan oligosaccharide. *Plant Physiology* 75:295-297.

(31) Ishii, T., Shimizu, K. 2001 Chemistry of Cell Wall Polysaccharides. In: *Wood and Cellulosic Chemistry* Hon, D. N.-S., Shiraishi, N., Eds., Marcel Dekker, Inc., New York 175-212.

(32) Rowell, R. M., Pettersen, R., Han, J. S., Rowell, J. S., Tshabalala, M. A. 2005 Cell Wall Chemistry. In: *Handbook of Wood Chemistry and Wood Composites* Rowell, R. M., Ed., CRC Press, Boca Raton, London, New York 35-74.

(33) Teleman, A., Nordström, M., Tenkanen, M., Jacobs, A., Dahlman, O. 2003 Isolation and characterization of O-acetylated glucomannans from aspen and birch wood. *Carbohydrate Research* 338(6):525-534.

(34) Aspinall, G. O., Sturgeon, R. J. 1957 Cereal gums. Part II. The constitution of an araboxylan from rye flour. *Journal of the Chemical Society*:4469-4471.

(35) Timell, T. E. 1964 Wood hemicelluloses: Part l. *Advances in Carbohydrate Chemistry and Biochemistry* 19:247.

(36) Höije, A., Sandström, C., Roubroeks, J. P., Andersson, R., Gohil, S., Gatenholm, P. 2006 Evidence for the presence of 2-O-β-D-xylopyranosyl-α-L-arabinofuranose side chains in barley husk arabinoxylan. *Carbohydrate Research* 341:2959-2966.

(37) Fincher, G. B., Stone, B. A. 1986 Cell walls and their components in cereal grain technology. In: *Advances in Cereal Science and Technology* Pomeranz, Y., Ed., American Association of Cereal Chemists Inc., St. Paul 207-295.

(38) Saastamoinen, M., Plaami, S., Kumpulainen, J. 1989 Pentosan and β-glucan content of Finnish winter rye varieties as compared with rye of six other countries *Journal of Cereal Science* 10(3):199-207.

(39) Åman, P., Hesselman, K. 1984 Analysis of starch and other main constituents of cereal grains. *Swedish Journal of Agricultural Research* 14:135-139.

(40) Bengtsson, S., Åman, P. 1990 Isolation and chemical characterization of water-soluble arabinoxylans in rye grain. *Carbohydrate Polymers* 12(3):267-277.

(41) Hafrén, J. 1999 Ph. D. Thesis, Royal Institute of Technology.

(42) Edashige, Y., Ishii, T., Hiroi, T., Fujii, T. 1995 Structural Analysis of Polysaccharides of Primary Walls from Xylem Differentiating Zones of *Cryptomeria Japonica* D. Don. *Holzforschung* 49(3):197-202.

(43) Vincken, J.-P. 2003 If Homogalacturonan Were a Side Chain of Rhamnogalacturonan I. Implications for cell Wall Architecture. *Plant and Cell Physiology* 132:1781-1789.

(44) Hafrén, J., Westermark, U. 2001 Distribution of Acidic and Esterified Polygalacturonans in Sapwood of Spruce, Birch and Aspen. *Nordic Pulp & Paper Research Journal* 16(4):284-290.

(45) Hafrén, J., Daniel, G., Westermark, U. 2000 The Distribution of Acidic and Esterified Pectin in Cambium, Developing Xylem and Mature Xylem of *Pinus sylvestris*. *IAWA* 21(2):157-168.

(46) Ress, D. A. 1982 Polysaccharide conformation in solutions and gels-recent results on pectins. *Carbohydrate Polymers* 2:254-263.

(47) Harrak, H., Chamberland, H., Plante, M. 1999 A Proline-, Threonine-, and Glycine-Rich Protein Down-Regulated by Drought Is localized in the Cell Wall of Xylem Elements. *Plant and Cell Physiology* 121:557-564.

(48) Qi, X., Behrens, B. X., West, P. R., Mort, A. J. 1995 Solubilisation and Partial Characterization of Extensin Fragments from Cell Wall of Cotton Suspension Cultures. *Plant Physiology* 108:1691-1701.

(49) Terashima, N., Hafrén, J., Westermark, U., Xie, Y., Fukushima, K., Lapierre, C., Vanderhart, D. 1999 Proposed 3D structural model for softwood lignin.

10th International Symposium on Wood and Pulping Chemistry, Yokohama pp.106-109.

(50) Watanabe, T. 2003 Analysis of Native Bonds Between Lignin and Carbohydrate by Specific Chemical Reactions. In: *Association between lignin and carbohydrates in wood and other plant tissues* Koshijima, T., Watanabe, T., Eds., Springer-Verlag Berlin, Heidelberg 91-130.

(51) Core, H. A., Côté, W. A., Day, A. C. 1979 *Wood Structure and Identification* Syracuse University Press, New York 32.

(52) Brändström, J. 2002 Ph.D. Thesis, Swedish University of Agricultural Science.

(53) Higuchi, T. 1997 Biosynthesis of Wood Components. In: *Biochemistry and Molecular Biology of Wood* Timell, T. E., Ed., Springer-Verlag, Berlin, Heidelberg New York 93-262.

(54) Atalla, R. H. 1998 Cellulose and the Hemicelluloses: Patterns for the Assembly of Lignin. In: *Lignin and lignan biosynthesis* Lewis, N. G., Sarkanen, S., Eds., Am. Chem. Soc., Washington DC 172-179.

(55) Terashima, N. 1990 A New Mechanism for Formation of a Structurally Ordered Protolignin Macromolecule in the Cell Wall of Tree Xylem. *Journal of Pulp and Paper Science* 16(5):J150-J154.

(56) Whitney, S. E. C., Gidley, M. J. 1999 Roles of Cellulose and Xyloglucan in Determining the Mechanical Properties of Primary Plant Cell Walls. *Plant Physiology* 121:657-663.

(57) Lawoko, M., Henriksson, G., Gellerstadt, G. 2006 Characterisation of lignin-carbohydrate complexes (LCCs) of spruce wood (Picea abies L.) isolated with two methods. *Holzforschung* 60:156-161.

(58) Christiane, L. 2005 Ph. D. Thesis, Helsinki University of Technology.

(59) Terashima, N., Fukushima, K., He, L.-F., Takabe, K. 1993 Comprehensive model of the lignified plant cell wall. In: *Forage Cell Wall Structure and Digestibility* Jung, H. G., Buxton, D. R., Hatfield, R. D., Ralph, J., Eds., American society of agronomy, Madison 247-270.

(60) Saxena, I. M., Brown, R. M., Jr. 2007 A Perspective on the Assembly of Cellulose-Synthesizing Complexes: Possible Role of KORRIGAN and Microtubules in Cellulose Synthesis in Plants. In: *Cellulose: Molecular and*

Structural Biology Brown, R. M. J., Saxena, I. M., Eds., Springer, Dordrecht 169-181.

(61) Hosoo, Y., Imai, T., Yoshida, M. 2005 Ultrastructural Investigations of Diurnal Periodicity in Cell Wall Formation of Conifer Tracheids. *Bulletin of the Faculty of Agriculture, Niigata University* 57(2):63-69.

(62) Fukushima, K., Terashima, N. 1991 Heterogeneity in Formation of Lignin. XIV. Formation and Structure of Lignin in Differentiating Xylem of *Ginkgo biloba*. *Holzforscung* 45:87-94.

(63) Ruel, K., Barnoud, F., Goring, D. A. I. 1978 Lamellation in the S2 layer of softwood tracheids as demonstrated by scanning transmission electron microscopy. *Wood Science and Technology* 12:287-291.

(64) Mark, R. E. 1972 Mechanical Behaviour of the Molecular Components of Fibres. In: *Theory and design of wood and fiber composite materials* Jayne, B. A., Ed., Syracuse University Press, Syracuse 49.

(65) Page, D. H. 1976 A note on the cell-wall structure of softwood tracheids. *Wood and Fiber* 7:246-248.

(66) Johnsson, K. G., Overend, R. P. 1991 Lignin-carbohydrate complexes from Populus deltides I. Purification and characterization. *Holzforschung* 45:469-475.

(67) Åkerholm, M., Salmén, L. 2001 Interactions between wood polymers studied by dynamic FT-IR spectroscopy. *Polymer* 42(3):963-969.

(68) Åkerholm, M. 2003 Ph.D. Thesis, Royal Institute of Technology.

(69) Karlsson, O., Westermark, U. 1996 Evidence for Chemical Bonds Between Lignin and Cellulose in Kraft Pulps. *Journal of Pulp and Paper Science* 22(10):397-401.

(70) Lundqvist, K., Simonson, R., Tingsvik, K. 1983 Lignin Carbohydrate Linkages in Milled Wood Lignin Preparations from Spruce Wood. *Svensk Papperstidning* 86(6):R44-R47.

(71) Eriksson, Ö., Goring, D. A. I., Lindgren, B. O. 1980 Structural Studies on the Chemical Bonds between Lignins and Carbohydrates in Spruce Wood. *Wood Science and Technology* 14(4):267-279.

(72) Hinterstoisser, B., Åkerholm, M., Salmén, L. 2001 Effect of fiber orientation in dynamic FTIR study on native cellulose. *Carbohydrate Research* 334:27-37.

(73) Mark, R. E. 1967 *Cell wall mechanics of tracheids* Yale University Press, London.

(74) Simonović, J., Stevanic, J. S., Djikanović, D., Salmén, L., Radotić, K. 2011 Cell wall polymers orientation in branches of hardwood and softwood - a polarized FTIR study. - *submitted to Macromolecular bioscience*.

(75) Olsson, A.-M., Bjurhager, I., Gerber, L., Sundberg, B., Salmén, L. 2011 Ultra-structural organisation of cell wall polymers in normal and tension wood of aspen revealed by polarisation FTIR microscopy. *Planta* 233 - in press (on-line publication: DOI 10.1007/s00425-011-1384-1).

(76) Salmén, L., Olsson, A.-M., Stevanic, J. S., Simonović, J., Radotić, K. 2011 Structural organisation of the wood polymers in the wood fibre structure. *The 16th ISWFPC*, Tianjin - in press.

(77) Jurasek, L. 1998 Molecular Modelling of Fibre Walls. *Journal of Pulp and Paper Science* 24(7):209-212.

(78) Atalla, R. H., Agarwal, U. P. 1985 Raman Microprobe Evidence for Lignin Orientation in the Cell Walls of Native Woody Tissue. *Science* 227:636-638.

(79) Åkerholm, M., Salmén, L. 2003 The oriented structure of lignin and its viscoelastic properties studied by static and dynamic FT-IR spectroscopy. *Holzforschung* 57(5):459-465.

(80) Leopold, B. 1961 Chemical composition and physical properties of wood fibers II. Alkali extraction of holocellulose fibers from loblolly pine. *Tappi* 44(3):232-235.

(81) Horii, F. 2001 Structure of cellulose: Recent Developments in Its Characterization. In: *Wood and Cellulosic Chemistry* Hon, D. N.-S., Shiraishi, N., Eds., Marcel Dekker, Inc., New York 83-107.

(82) Brown, R. M., Jr., Willison, J. H. M., Richardson, C. L. 1976 Cellulose biosynthesis in *Acetobacter xylinum*: visualization of the site of synthesis and direct measurement of the *in vivo* process. *PNAS* 73(12):4565-4569.

(83) Zaar, K. 1977 The biogenesis by cellulose by *Axetobacter xylinum*. *Cytobiologie* 16:1-15.

(84) Bielecki, S., Krystynowicz, A., Turkiewicz, M., Kalinowska, H. 2005 Bacterial cellulose. In: *Polysaccharides and polyamides in the food industry: properties, production, and patents* Steinbüchel, A., Rhee, S. K., Eds., Wiley-VCH, Weinheim 37-46.

(85) Czaja, W. K., Young, D. J., Kawecki, M., Brown, R. M., Jr 2007 The Future Prospects of Microbial Cellulose in Biomedical Applications. *Biomacromolecules* 8(1):1-12.

(86) Jonas, R., Farah, L. F. 1998 Production and application of microbial cellulose. *Polymer Degradation and Stability* 59(1-3):101-106.

(87) Czaja, W., Krystynowicz, A., Bielecki, S., Brown, R. M., Jr 2006 Microbial cellulose - the natural power to heal wounds. *Biomaterials* 27:145-151.

(88) Czaja, W., Krystynowicz, A., Kawecki, M., Wysota, K., Sakiel, S., Wroblewski, P., Glik, J., Nowak, M., Bielecki, S. 2007 Biomedical applications of microbial cellulose in burn wound recovery. In: *Cellulose: Molecular and Structural Biology* Brown, R. M., Jr., Saxena, I. M., Eds., Springer, Dordrecht 307-321.

(89) Nishi, Y., Uryu, M., Yamanaka, S., Watanabe, K., Kitamura, N., Iguchi, M., Mitsuhashi, S. 1990 The structure and mechanical properties of sheet prepared from bacterial cellulose. Part 2: improvement of the mechanical properties of sheets and their aplicability to diaphragms of electroacustic transducers. *Journal of Material Science* 25(6):2997-3001.

(90) Czaja, W., Romanovicz, D., Brown, R. M., Jr 2004 Structural investigations of microbial cellulose produced in stationary and agitated culture. *Cellulose* 11:403-411.

(91) Uhlin, K. I., Atalla, R. H., Thompson, N. S. 1995 Influence of Hemicelluloses on the Aggregation Patterns of Bacterial Cellulose. *Cellulose* 2(2):129-144.

(92) Åkerholm, M., Hinterstoisser, B., Salmén, L. 2004 Characterization of the crystalline structure of cellulose using static and dynamic FT-IR spectroscopy. *Carbohydrate Research* 339(3):569-578.

(93) Brown, R. M., Jr 1989 Bacterial cellulose. In: *Cellulose: Structural and Functional Aspects* Kennedy, J. F., Phillips, G. O., Williams, P. A., Eds., Ellis Horwood Ltd., Chichester, New York 145-151.

(94) Wilfför, S., Rehn, P., Sundberg, A., Sundberg, K., Holmbom, B. 2003 Recovery of water-soluble acetylgalactoglucomannans from mechanical pulp of spruce. *Tappi Journal* 2(11):27-32.

(95) Xu, C., Willför, S., Sundberg, K., Petterson, C., Holmbom, B. 2006 Physico-chemical characterisation of spruce galactoglucomannan solutions: stability,

surface, activity and rheology. *Cellulose Chemistry and Technology* 41(1):51-62.

(96) Pääkkö, M., Ankerfors, M., Kosonen, H., Nykänen, A., Ahola, S., Österberg, M., Roukolainen, J., Laine, J., Larsson, P. T., Ikkala, O., Lindström, T. 2007 Enzymatic Hydrolysis Combined with Mechanical Shearing and High-Pressure Homogenization for Nanoscale Cellulose Fibrils and Strong Gels. *Biomacromolecules* 8:1934-1941.

(97) Svagan, A. J., S., A. S. M. A., Berglund, L. A. 2007 Biomimetic Polysaccharide Nanocomposites of High Cellulose Content and High Toughness. *Biomacromolecules* 8:2556-2563.

(98) Hult, E.-L., Larsson, P. T., Iversen, T. 2001 Cellulose fibril aggregation - An inherent property of kraft pulps. *Polymer* 42(8):3309-3314.

(99) Siró, I., Plackett, D. 2010 Microfibrillated cellulose and new nanocomposite materials: a review. *Cellulose* 17:459-494.

(100) Turbak, A. F., Snyder, F. W., Sandberg, K. R. 1983 Microfibrillated cellulose, a new cellulose product: properties, uses, and commercial potential. *Journal of Applied Polymer Science: Applied Polymer Symposium* 37:815-827.

(101) Herrick, F. W., Casebier, R. L., Hamilton, J. K., Sandberg, K. R. 1983 Microfibrillated cellulose: morphology and accessibility. *Journal of Applied Polymer Science: Applied Polymer Symposium* 37:797-813.

(102) Wågberg, L., Winter, L., Ödberg, L., Lindström, T. 1987 On the charge stoichiometry upon adsorption of a cationic polyelectrolyte on cellulosic materials *Colloids and Surfaces* 27(1-3):163-173.

(103) Wågberg, L., Decher, G., Norgren, M., Lindström, T., Ankerfors, M., Axnäs, K. 2008 The Build-Up of Polyelectrolyte Multilayers of Microfibrillated Cellulose and Cationic Polyelectrolytes. *Langmuir* 24:784-795.

(104) Plackett, D., Anturi, H., Hedenqvist, M., Ankefors, M., Gällstedt, M., Lindström, T., Siró, I. 2010 Physical Properties and Morphology of Films Prepared from Microfibrillated Cellulose in Conbination with Amylopectin. *Journal of Applied Polymer Science* 117:3601-3609.

(105) Siró, I., Plackett, D., Hedenqvist, M., Ankefors, M., Lindström, T. 2011 Highly Transparent Films from Carboxymethylated Microfibrillated Cellulose: The Effect of Multiple Homogenisation Steps on Key Properties. *Journal of Applied Polymer Science* 119:2652-2660.

(106) Skoog, D. A., Leary, J. J. 1992 *Principles of Instrumental Analysis* Saunders College Publishing, Orlando 113-270.

(107) Noda, I., Dowrey, A. E., Marcott, C. 1987 Characterization of polymers using polarization-modulation infrared techniques: dynamic infrared linear dichroism (DIRLD) spectroscopy. In: *Characterization of polymers* Ishida, H., Ed., Plenum, New York 33-59.

(108) Noda, I., Dowrey, A. E., Marcott, C. 1983 Dynamic Infrared Linear Dichroism of Polymer Films under Oscillatory Deformation. *Journal of Polymer Science: Polymer Letters Edition* 21:99-103.

(109) Noda, I., Dowrey, A. E., Marcott, C. 1988 A Spectrometer for Measuring Time-Resolved Infrared Linear Dichroism Induced by a Small-Amplitude Oscillatory Strain. *Applied Spectroscopy* 42(2):203-216.

(110) Noda, I., Dowrey, A. E., Marcott, C. 1999 Two-Dimensional Infrared (2D IR) Spectroscopy. In: *Modern Polymer Spectroscopy* Zerbi, G., Ed., Wiley-VCH, Weinheim 1-32.

(111) Noda, I. 1989 Two-Dimensional Infrared Spectroscopy. *Journal of American Chemical Society* 111:8116-8118.

(112) Noda, I. 1990 Two-Dimensional Infrared (2D IR) Spectroscopy: Theory and Applications. *Applied Spectroscopy* 44(4):550-561.

(113) Budevska, B. O., Manning, C. J., Griffith, P. R. 1994 Comparison of Two-Dimensional Power and Phase Spectra Generated from Sample Modulation Step Scan FT-IR Experiments. *Applied Spectroscopy* 48(12):1556-1559.

(114) Budevska, B. O., Manning, C. J., Griffiths, P. R., Roginski, R. T. 1993 Step-Scan Fourier Transform Infrared Study on the Effect of Dynamic Strain on Isotactic Polypropylene. *Applied Spectroscopy* 47(11):1843-1851.

(115) Noda, I. 1993 Generalized Two-Dimensional Correlation Method Applicable to Infrared, Raman, and Other Types of Spectroscopy. *Applied Spectroscopy* 47(9):1329-1336.

(116) Salmén, L., Hagen, R. 2001 Viscoelastic properties. In: *Handbook of physical testing of paper* Mark, R. E., C C Habeger, J., Borch, J., Lyne, M. B., Eds., Marcel Dekker, New York 77-113.

(117) Levine, H., Slade, L. 1988 Water as plasticizer: physico-chemical aspects of low moisture polymeric system. In: *Water Science Reviews* Franks, F., Ed., Cambridge University Press, Cambridge 79-185.

(118) Salmén, L., Back, E. L. 1980 Moisture-dependent thermal softening of paper, evaluated by its elastic modulus. *Tappi* 63(6):117-120.

(119) Bradley, S. A., Carr, S. H. 1976 Mechanical Loss Processes in Polysaccharides. *Journal of Polymer Science: Polymer Physics* 14:111-124.

(120) Almgren, K. 2007 Lic. Thesis, Royal Institute of Technology.

(121) Åkerholm, M., Salmén, L. 2002 Orientation and dynamic behavior of lignin in the cell wall. *Seventh European Workshop on Lignocellulosics and Pulp*, Åbo pp.27-30.

(122) Collier, W., Kalasinsky, V. F., Schulz, T. P. 1997 Infrared study of lignin: Assignment of methoxyl C-H bending and stretching bands. *Holzforschung* 51(2):167-168.

(123) Collier, W. E., Schultz, T. P., Kalasinsky, V. F. 1992 Infrared Study of Lignin: Reexamination of Aryl-Alkyl Ether C-O Stretching Peak Assignment. *Holzforschung* 46(6):523-528.

(124) Faix, O. 1991 Classification of Lignins from Different Botanical Origins by FTIR Spectroscopy. *Holzforschung* 45(Supplement):21-27.

(125) Agarwal, U. P., Ralph, S. A. 1997 FT-Raman Spectroscopy of Wood: Identifying Contributions of Lignin and Carbohydrate Polymers in the Spectrum of Black Spruce (*Picea mariana*). *Applied Spectroscopy* 51(11):1648-1655.

(126) Agarwal, U. P., Ralph, S. A., Atalla, R. H. 1997 FT Raman spectroscopic study of softwood lignin. *9th International symposium on wood and pulping chemistry (ISWPC)*, Montreal pp.8-1-8-4.

(127) Åkerholm, M. 2003 Ph. D. Thesis, Royal Institute of Technology.

(128) Chen, L., Wilson, H., McCann, M. C. 1997 Infra-red microspectroscopy of hydrated biological systems: design and construction of a new cell with atmospheric control for the study of plant cell walls. *Journal of Microscopy* 188:62-71.

(129) Günzeler, H., Gremlich, H.-U. 2002 *IR Spectroscopy* Wiley-VCH, Weinheim 171-278.

(130) Faix, O. 1986 Investigation of lignin polymer models (DHP's) by FTIR spectroscopy. *Holzforschung* 40:273-280.

(131) Liang, C. Y., Basset, K. H., McGinnes, E. A., Marchessault, R. H. 1960 Infrared Spectra of Crystalline Polysaccharides; VII. Thin Wood Sections. *Tappi* 43(12):1017-1024.

(132) Marchessault, R. H. 1962 Application of Infra-Red Spectroscopy to Cellulose and Wood Polysaccharides. *Pure and Applied Chemistry* 5:107-129.

(133) Marchessault, R. H., Liang, C. Y. 1962 The Infrared Spectra of Crystalline Polysaccharides. VIII. Xylans. *Journal of Polymer Science* 59:357-378.

(134) Boyd, J. D. 1982 An anatomical explanation for visco-elastic and mechanosorptive creep in wood, and effects of loading rate on strength. In: *New perspective in wood anatomy* Baas, P., Ed., Martinus Nijhoff/Dr W Junk, La Hague 171-222.

(135) St-Germain, F. G. T., Gray, D. G. 1987 Photoacoustic Fourier Transform Infrared Spectroscopic Study of Mechanical Pulp Brightening. *Journal of Wood Chemistry and Technology* 7(1):33-50.

(136) Olsson, A.-M., Salmén, L. 1997 Humidity and Temperature Affecting Hemicellulose Softening in Wood. *International Conference of COST Action E8. Mechanical Performance of Wood and Wood Products. Wood-water relation*, Copenhagen pp.269-279.

(137) Olsson, A.-M., Salmén, L. 2004 The softening behaviour of hemicelluloses related to moisture. *ACS Symp ser.864 Hemicelluloses: Science and technology*, Washington pp.184-197.

(138) Almond, A., Sheehan, J. K. 2003 Predicting the molecular shape of polysaccharides from dynamic interactions with water. *Glycobiology* 13(4):255-264.

(139) Bishop, C. T. 1953 Crystalline Xylans from Straws. *Canadian Journal of Chemistry* 31:793-800.

(140) Sternemalm, E., Höije, A., Gatenholm, P. 2008 Effect of arabinose on the material properties of arabinoxylan films. *Carbohydrate Research* 343:753-757.

(141) Andrewartha, K. A., Phillips, D. R., Stone, B. A. 1979 Solution properties of wheat-flour arabinoxylans and enzymatically modified arabinoxylans. *Carbohydrate Research* 77:191-204.

(142) Mikkonen, K., Mathew, A. P., Pirkkalainen, K., Serimaa, R., Xu, C., Willför, S., Oksman, K., Tenkanen, M. 2010 Glucomannan composite films with cellulose nanowhiskers. *Cellulose* 17:69-81.

(143) Nordqvist, D., Idermark, J., Hedenqvist, M. S., Gällstedt, M., Ankefors, M., Lindström, T. 2007 Enhancement of the wet properties of transparent chitosan-acetic-acid-salt films using microfibrillated cellulose. *Biomacromolecules* 8(8):2398-2403.